



Cite this: *RSC Adv.*, 2022, 12, 13950

# Water-soluble optical sensors: keys to detect aluminium in biological environment

Ajmal Roshan Unniram Parambil, <sup>\*abc</sup> Kavyashree P.,<sup>†a</sup> Akshay Silswal<sup>†a</sup> and Apurba Lal Koner <sup>\*a</sup>

Metal ion plays a critical role from enzyme catalysis to cellular health and functions. The concentration of metal ions in a living system is highly regulated. Among the biologically relevant metal ions, the role and toxicity of aluminium in specific biological functions have been getting significant attention in recent years. The interaction of aluminium and the living system is unavoidable due to its high earth crust abundance, and the long-term exposure to aluminium can be fatal for life. The adverse  $\text{Al}^{3+}$  toxicity effects in humans result in various diseases ranging from cancers to neurogenetic disorders. Several  $\text{Al}^{3+}$  ions sensors have been developed over the past decades using the optical responses of synthesized molecules. However, only limited numbers of water-soluble optical sensors have been reported so far. In this review, we have confined our discussion to water-soluble  $\text{Al}^{3+}$  ions detection using optical methods and their utility for live-cell imaging and real-life application.

Received 23rd February 2022  
Accepted 22nd April 2022

DOI: 10.1039/d2ra01222g

rsc.li/rsc-advances

<sup>a</sup>Bionanotechnology Lab, Department of Chemistry, Indian Institute of Science Education and Research Bhopal, Bhopal Bypass Road, Bhauri, 462066 Bhopal, Madhya Pradesh, India. E-mail: akoner@iiserb.ac.in

<sup>b</sup>Department of Chemistry, University of Basel, 4058 Basel, Switzerland. E-mail: ajmalrup@gmail.com

<sup>c</sup>Institute of Chemistry and Bioanalytics, School of Life Sciences, University of Applied Sciences and Arts Northwestern Switzerland, 4132 Muttenz, Switzerland

<sup>†</sup> Contributed equally.



**Left to right: Apurba Lal Koner, Akshay Silswal, Kavyashree P. and Ajmal Roshan Unniram Parambil** Mr Ajmal Roshan U P completed his integrated BS-MS dual degree in 2021 with a major in Chemistry from IISER Bhopal. He worked on developing rhodamine-based trivalent metal ion sensors for his Master's thesis under the supervision of Dr Apurba Lal Koner. He is currently pursuing a PhD at the University of Basel on developing designer nanocrystals for the fabrication of molecularly precise 2D and 3D metal-organic frameworks.

Ms Kavyashree P. completed her MSc in organic chemistry from Mangalore University, Mangalore in 2017. In the same year, she started her doctoral studies under the supervision of Dr Apurba Lal Koner, IISER Bhopal. Her research interest is in the synthesis of styryl-based fluorescent molecules and exploring their applications for the detection of different analytes.

Mr Akshay Silswal received his MSc degree from Hemwati Nandan Bhaguna Garhwal University in 2016. Currently, he is pursuing his doctoral research at IISER Bhopal. His research interest lies in developing fluorophores for targeting specific cellular organelles to understand their biophysics and sensing applications.

Dr Apurba Lal Koner is currently an Associate Professor at IISER Bhopal. He obtained his PhD in Chemistry from Jacobs University Bremen, Germany. After postdoctoral work at the University of Oxford, he joined IISER Bhopal as a faculty member in the Department of Chemistry in 2012. One of his current research interests lies in the design and synthesis of novel fluorescent probes for sensing and fluorescence imaging.



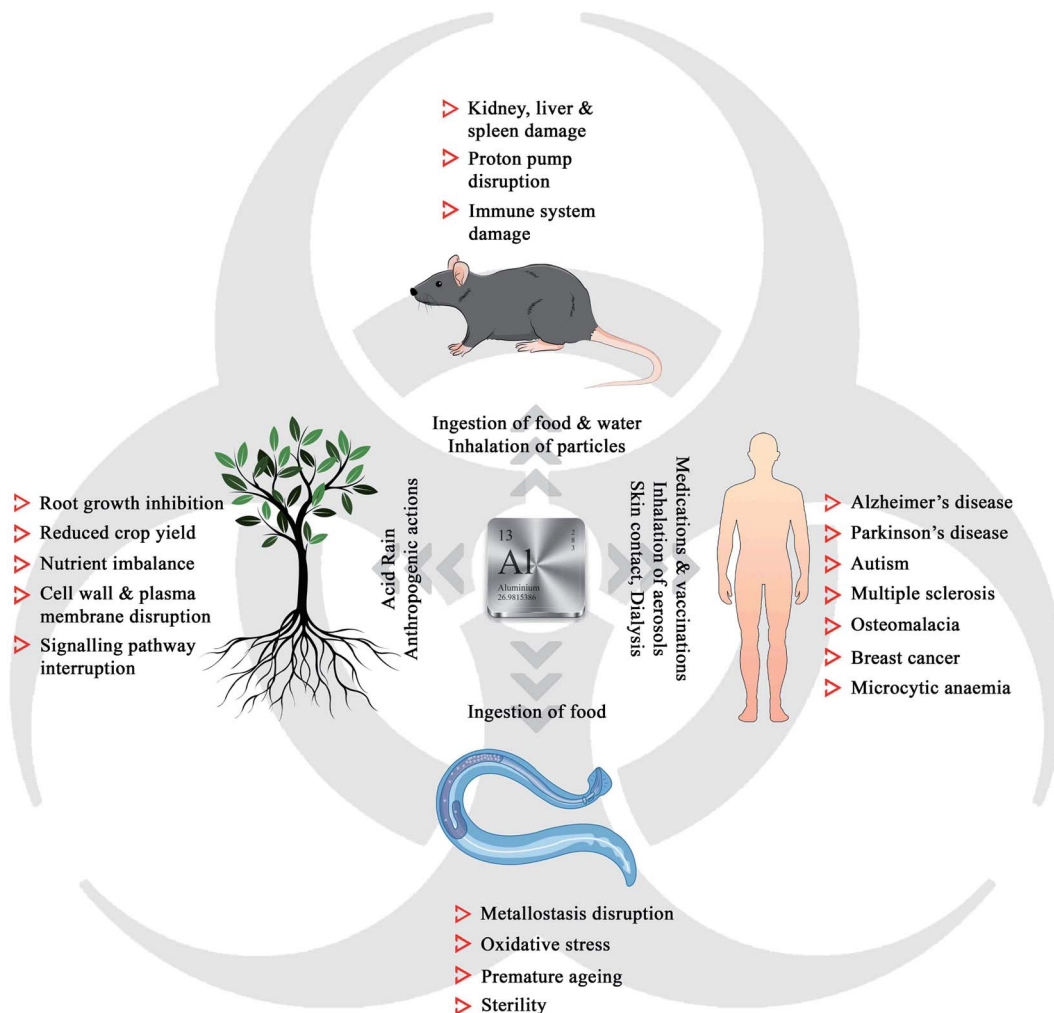


Fig. 1 Toxic effects of  $\text{Al}^{3+}$  in the biotic community.

## 1. Introduction

The history of humans and metals goes back to centuries, both physiologically and economically, as most of metals have played a significant role in the progress of civilization.<sup>1</sup> Aluminium, being the most abundant metal and the third most element on Earth (8.1% of Earth's mass), is widely used in our daily life, starting from medicines to aircraft. The presence of non-essential aluminium in life forms leaves the question of toxicity in biological systems.<sup>2,3</sup> Rigorous research in this field has revealed that aluminium exposure and intake is detrimental to plants, model organisms, and humans (Fig. 1).<sup>4,5</sup>

Aluminium exists in different forms, such as minerals (aluminium oxides and aluminosilicates), as well as organic and inorganic precipitates, making it an essential component of mineral soil. Though naturally occurring silicates and oxides are harmless, soil acidification due to acid rain and anthropogenic actions can trigger the leaching of aluminium, leading to damage to the growth of plants.<sup>6</sup> The phytotoxicity of  $\text{Al}^{3+}$  includes root growth inhibition, reduced crop yield, cell wall damage, plasma membrane disruption, signalling pathway

interruption, and nutrient imbalance.<sup>7–16</sup> Aluminium is easily accessible to both animal and human populations through the inhalation of particles and aerosols, ingestion of food and water, medications, vaccinations, skin contact, dialysis, and infusions.<sup>17</sup> Recent research in neurobiology has revealed that aluminium could act as a neurotoxin, damaging the nerve tissues, which is associated with several neurogenetic disorders such as Alzheimer's disease, Parkinson's disease, autism, and multiple sclerosis.<sup>18</sup> Chronic exposure to aluminium to the model organism *Caenorhabditis elegans* led to the disruption of metallostasis, oxidative stress, premature aging, and sterility.<sup>19</sup> Kamalov *et al.* reported that an environmentally relevant concentration of aluminium could damage the thymocytes and lymphocytes and gradually the immune system in mice.<sup>20</sup> The adverse effects of aluminium urge the detailed investigation on the detection, selective removal, or conversion of  $\text{Al}^{3+}$  to non-toxic species, which are highly necessary to control its concentration below the ecotoxic levels in the biosphere.

To date, a variety of techniques such as inductively coupled plasma emission spectroscopy (ICPES), atomic fluorescence spectroscopy (AFS), and X-ray photoelectron spectrometry (XPS)

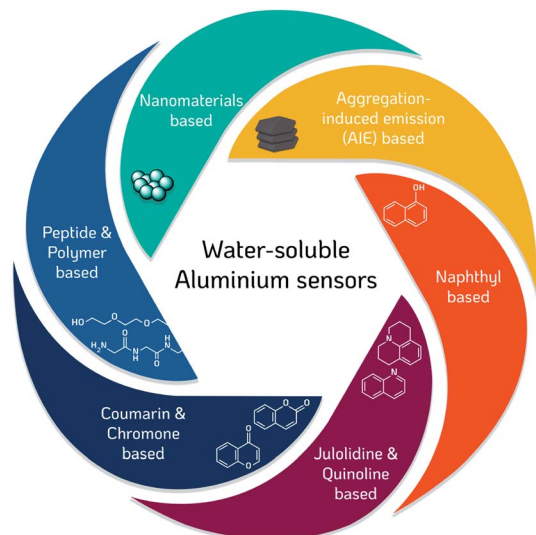


Fig. 2 Different classes of water-soluble aluminium sensors.

have been developed for  $\text{Al}^{3+}$  sensing. Despite their high sensitivity and selectivity, complicated instrumentation, high cost, and tricky operation have hindered their practical utility. In this scenario, the development of fluorescent probe-based chemosensors is an active research field that has garnered tremendous momentum over the past few years.<sup>21–26</sup> The use of optical probes is considered as the most convenient, inexpensive, effective, and rapid method for the detection of  $\text{Al}^{3+}$ . Several probes based on rhodamine,<sup>27,28</sup> naphthol,<sup>29</sup> fluorescein,<sup>30</sup> and spirobenzopyran<sup>31</sup> have been synthesized to detect  $\text{Al}^{3+}$  cations exploiting their color and fluorescence properties. Recently, Prof. Roy has comprehensively reviewed aluminium sensors derived from 2-hydroxy-1-naphthaldehyde, salicylaldehyde, rhodamine, coumarin, and different metal-based-metal-organic frameworks (MOFs).<sup>32</sup> However, most of the reported chemosensors require mixed aqueous–organic solvent systems due to their poor solubility in polar buffered/aqueous medium. Besides their poor solubility in water, many fluorescent sensors are being used to detect  $\text{Al}^{3+}$  in live cells, *Drosophila melanogaster*, *Escherichia coli*, zebrafish, rice seedlings, etc.<sup>33–39</sup> However, the utilization of organic solvents for cellular imaging can destroy the cells, causing inaccurate sensing of intracellular  $\text{Al}^{3+}$ . Therefore, the development of water-soluble fluorescent  $\text{Al}^{3+}$  sensors would effectively enhance the efficiency of detection to the next level.

In this review, we will attempt to provide a clear picture on different classes of water-soluble aluminium sensing probes based on colorimetric and fluorometric detection (Fig. 2 and Table 1). We limit our discussion to optical sensors that can act in aqueous solutions with organic solvents less than 2%. Rather than focusing on the synthetic ways, we have discussed the efficiency, spectroscopic properties, and practical applications, deeply examined the sensing mechanisms, compared the selectivity, and detection levels of several probes, and highlight the characteristic requirements of a bio-applicable aluminium detecting fluorescent probe.

## 2. Results and discussions

### 2.1 Naphthyl-based sensors

From the historical viewpoint, the ultra-sensitive determination of  $\text{Al}^{3+}$  through naphthalene derivative dates to 1994.<sup>40</sup> Over the years, the endeavor of organic synthesis judiciously tailored naphthalene into numerous fluorogenic molecular architectures for metal sensing. 2-Hydroxy-1-naphthaldehyde or 1-hydroxy-2-naphthaldehyde (HN) is a vastly explored derivative of naphthalene, and has poor quantum yield, shorter fluorescence lifetime,<sup>41</sup> and lower cost.<sup>42</sup> In addition, successful condensation with appropriate amines afforded Schiff-bases, where the imine nitrogen and naphthol hydroxy behave as hard donors to efficiently coordinate the hard acid  $\text{Al}^{3+}$ .<sup>43,44</sup> Also, the rational choice of amine counterparts can alter the binding sites to furnish strong interaction with the aluminium ion. The distinguished selective chelation with  $\text{Al}^{3+}$  augmented the fluorescence intensity of weakly emissive imine chemosensors. Mechanistically, it involves arresting the photoinduced electron transfer (PET) process and isomerization around the  $\text{C}=\text{N}$  bond, exhibiting a chelation enhanced fluorescence (CHEF) effect. Therefore, elegantly developed NH-derived Schiff-bases emerged as promising sensors for  $\text{Al}^{3+}$  recognition. Herein, we are dealing with some pertinent examples of this category.

In 1994, Baksi and coworkers employed chromotropic acid (4,5-dihydroxynaphthalene-2,7-disulfonic acid; **1**, Scheme 1) as an ultra-sensitive fluorometric reagent for the selective recognition of  $\text{Al}^{3+}$  in nano-trace levels.<sup>40</sup> The presence of donor–acceptor moieties at 1,6-position made the probe fluorescent. However, discrepancies related to the absence of wide-range studies on the increase in emission intensity with  $\text{Al}^{3+}$  ion, binding stoichiometry, and use of acetic acid/acetate buffer (pH = 4.0) made Bardez and coworkers revisit the sensing properties of **1** in 2004.<sup>45</sup> An increase in absorption at 360 nm (Fig. 3a) and a fluorescence enhancement at 387 nm (Fig. 3b) was observed upon  $\text{Al}^{3+}$  addition. A detailed study by the authors complemented the previous reports on **1** by forming a 1 : 1 complex with a limit of detection of  $0.65 \mu\text{g L}^{-1}$  at pH = 4.0. They have also demonstrated the application of the probe in determining the  $\text{Al}^{3+}$  in different tap water samples. The obtained results were compared with the outcomes attained from the atomic absorption spectroscopy (AAS). However, the methodology is not selective to  $\text{Al}^{3+}$ , when the interfering ion is  $\text{Ga}^{3+}$ .

Later, in 2012, Chattopadhyay and coworkers illustrated an efficient dual-mode sensing of  $\text{Al}^{3+}$  through colorimetric and fluorescence turn-on behavior of chemosensor **2** (Scheme 1) in HEPES buffer (DMSO/water: 1/100) of pH 7.4.<sup>46</sup> The synthesized Schiff-base probe **2** comprises a naphthalene unit behaving as a signalling moiety, whereas the functional groups – hydroxyl and imine provide the chelating site for the selective binding of  $\text{Al}^{3+}$ . The complexation of the probe with  $\text{Al}^{3+}$  rendered a decrease in the absorbance at 335 and 392 nm with concomitant enhanced absorption at 412 nm (Fig. 3c). The remarkable changes in the absorption spectra facilitated a visible color change of the solution from yellow to reddish-yellow, providing naked-eye detection (Fig. 3c; inset image).



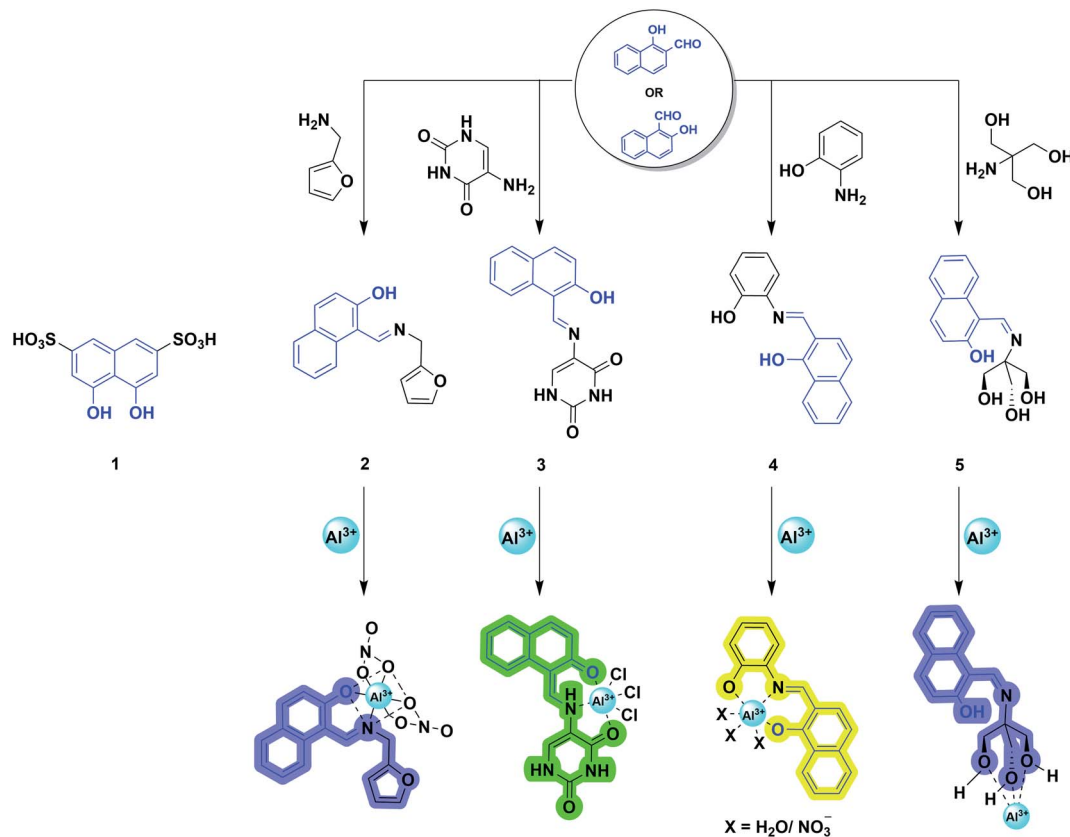


**Table 1** Reported water-soluble  $\text{Al}^{3+}$  sensor utilizing optical responses

	Sensor method	Detection	Solvent	Wavelength/nm		LOD	$K/\text{M}^{-1}$	Stoichiometry <sup>a</sup>	Applications	Reference
				$\lambda_{\text{ex}}$	$\lambda_{\text{em}}$					
Naphthyl based sensors	1	Fluorometric	Water (pH 4.0)	360	387	0.65 $\mu\text{g L}^{-1}$	—	1 : 1	Water samples	40,45
	2	Fluorometric & colorimetric	HEPES buffer (pH 7.4) (water/DMSO 100 : 1)	355	470	0.603 $\mu\text{M}$	$0.35 \times 10^5$	1 : 1	Live-cell imaging (HeLa cells)	46
	3	Fluorometric & colorimetric	Water	450	490/495	1 $\mu\text{M}$	$3.148 \times 10^4$	1 : 1	—	47
	4	Fluorometric	Bis-tris buffer (pH 7.0)	450	490/515	0.13 $\mu\text{M}$	$2.5 \times 10^3$	1 : 1	Live-cell imaging (HeLa cells)	48
	5	Fluorometric & colorimetric	HEPES buffer (pH 7.0)	320	380	0.1 $\mu\text{M}$	$1.19 \times 10^8$	1 : 1	—	49
	6	Fluorometric	Water	420	575	0.056 $\mu\text{M}$	$0.21 \times 10^2 \text{ M}^{-2}$	2 : 1	—	50
Julolidine & quinoline based sensors	7	Fluorometric	Tris buffer (10 mM, pH 7.0)	450	482	0.13 $\mu\text{M}$	$1 \times 10^7$	1 : 1	Live-cell imaging (HeLa cells)	51
	8	Fluorometric	Bis-tris buffer (10 mM, pH 7.0)	440	487	1.12 $\mu\text{M}$	$2.1 \times 10^5$	1 : 1	Live-cell imaging (human dermal fibroblast)	52
	9	Fluorometric & colorimetric	99% Water/DMSO	403	487	54 nM	—	2 : 1	Aqueous solution and test paper	53
	10	Fluorometric	Tris-HCl (0.1 mM, pH 7.2)	334	445	336 nM	$4.2 \times 10^3$	1 : 1	—	54
Coumarin & chromone based sensors	11	Fluorometric	Tris-HCl (10 mM, pH 7.2)	335	450	66.5 nM	$9.5 \times 10^5$	2 : 1	—	58
	12	Fluorometric	$\text{H}_2\text{O}/\text{DMSO}$ (50 : 1)	387	~490	5.1 $\mu\text{M}$	$7.6 \times 10^3$	1 : 1	—	59
	13	Fluorometric	$\text{H}_2\text{O}/\text{DMSO}$ (50 : 1)	310	~455	3 $\mu\text{M}$	$2.9 \times 10^3$	1 : 1	—	59
	14	Fluorometric & colorimetric	Hexamine buffer (10 mM, pH 5.5)	380	536	230 nM	$2.1 \times 10^9$	2 : 1	—	66
Peptide-based sensors	15	Fluorometric	Hexamine buffer (10 mM, pH 5.5)	315	(516) <sup>b</sup>	195 nM	$1.84 \times 10^4$	1 : 1	—	67
	16	Fluorometric	Hexamine buffer (10 mM, pH 5.5)	315	(455) <sup>b</sup>	155 nM	$1.30 \times 10^4$	1 : 1	—	67
	17	Fluorometric	Water	345	435	9.67 nM	$1.76 \times 10^4$	1 : 1	Real water samples	70
	18	Fluorometric	Water	399	469	6.15 nM	$1.30 \times 10^5$	1 : 1	—	68
Nanomaterial based	19	Fluorometric	Water	367	447	4.05 nM	$6.39 \times 10^4$	2 : 1	Real water samples	69
	20	Colorimetric	Water	530/392	—	2.0 nM	$1.18 \times 10^5$	2 : 1	Live cell (mouse myeloma cells) and real water samples	71
	21	Fluorometric	$\text{H}_2\text{O}/\text{DMF}$ (99 : 1)	~290	390/500	677 nM	—	—	Soil samples	72
	22	Fluorometric & colorimetric	Water	510	650	20 $\mu\text{M}$	—	—	Live cell (normal lung AT II cells)	73
AIE based	23	Fluorometric	HEPES buffer (pH 7.4, 10 mM)	330	455	14 nM	—	1 : 1	Live cell imaging (A549 cells) and real water samples	74
	24	Fluorometric	HEPES buffer (pH 7, 10 mM)	363	511	153 nM	$1.99 \times 10^4$	1 : 1	Microfluidic setup for real water samples	75

<sup>a</sup> Receptor: analyte binding ratio. <sup>b</sup> Initial emission wavelength (blue-shifted emission wavelength).





Scheme 1 Structures of naphthyl-based  $\text{Al}^{3+}$  chemosensors (1, 2, 3, 4, and 5) and sensing mechanisms.

Also, the probe exhibited a remarkable increase in the emission intensity at 470 nm (Fig. 3d), with the lowest detection limit of  $6.03 \times 10^{-7}$  M and a strong binding constant of  $0.35 \times 10^5 \text{ M}^{-1}$ . The bidentate and mono-basic nature of the ligand in the rigid chelated product was supported by  $^1\text{H}$  NMR titration of the probe with  $\text{Al}^{3+}$  in  $\text{DMSO}-d_6$  and DFT calculations. Thus, mechanistically, a reduction in the internal charge transfer (ICT) and improved CHEF probably contributes to the selective detection of  $\text{Al}^{3+}$  via 1 : 1 complexation with 2. The authors also demonstrated the potential capability of the probe for the intracellular imaging of  $\text{Al}^{3+}$  in HeLa cells.

In the very next year, Singh and coworkers redesigned the probe 2 to construct a biologically interesting product 3 (Scheme 1)<sup>47</sup> where the furan-derivative amine counterpart was replaced by 5-aminouracil to form the imine moiety. The authors claimed that this is the first report on the Schiff-base of 5-aminouracil with NH for the sensing of  $\text{Al}^{3+}$  through the phenomenon of CHEF. In aqueous media, the keto tautomeric form of the probe selectively chelates with  $\text{Al}^{3+}$ , thus exhibiting an enhancement in the emission intensity at 495 nm (Fig. 4a). Nevertheless, the presence of other cationic species did not alter the fluorescence intensity of the probe. The formation of the stable 1 : 1 complex was established by Job's plot and electrospray ionization (ESI) mass analysis. Ligand 3 behaves as a tridentate Schiff-base by coordinating  $\text{Al}^{3+}$  via the carbonyl of uracil, imine nitrogen, and keto group on the naphthalene ring, as is evident from the  $^1\text{H}$  NMR studies. Further, the binding

constant and detection limit were determined to be  $(1.5 \pm 0.009) \times 10^5 \text{ M}^{-1}$  and 1.0  $\mu\text{M}$ , respectively.

Exploiting the similar Schiff-base approach, a novel phenol-naphthol hybrid chemosensor 4 (Scheme 1) was reported by Kim and coworkers in 2014.<sup>48</sup> The developed chemosensor distinguishes  $\text{Al}^{3+}$  and  $\text{CN}^-$  from other metal ions through fluorescence enhancement and quenching effect in bis-tris buffer and methanolic medium, respectively. A 100-fold increase in the emission intensity at 490 and 515 nm was observed with the gradual addition of 34 equiv.  $\text{Al}^{3+}$  (Fig. 4b). However, turn-on fluorescence feedback got significantly subdued in the presence of competing metal ions such as  $\text{Ag}^+$ ,  $\text{Cu}^{2+}$ ,  $\text{Cr}^{3+}$ , and  $\text{Fe}^{3+}$  (Fig. 4c). Mechanistically, 1 : 1 chelation with 4 inhibits the rotation of the aromatic rings around the imine moiety. This brings both the naphthol and phenol rings to the same plane and furnishes a conjugated system that enhances the emission intensity upon  $\text{Al}^{3+}$  binding. The stability constant of the complex and the lowest detection limit for aluminium ions were found to be  $2.5 \times 10^3 \text{ M}^{-1}$  and 0.13  $\mu\text{M}$ , respectively. In addition, the authors also illustrated the successful tracking of intracellular  $\text{Al}^{3+}$  in HeLa cells using 4 (Fig. 4d).

Utilizing the excellent sensing properties of HN, in the same year, Liu and coworkers illustrated the design and synthesis of another naphthol aldehyde-tris derivate molecular probe 5 (Scheme 1) for  $\text{Al}^{3+}$  detection.<sup>49</sup> The UV-Vis absorption spectra revealed a reduction in the O.D. value between 400–420 nm and



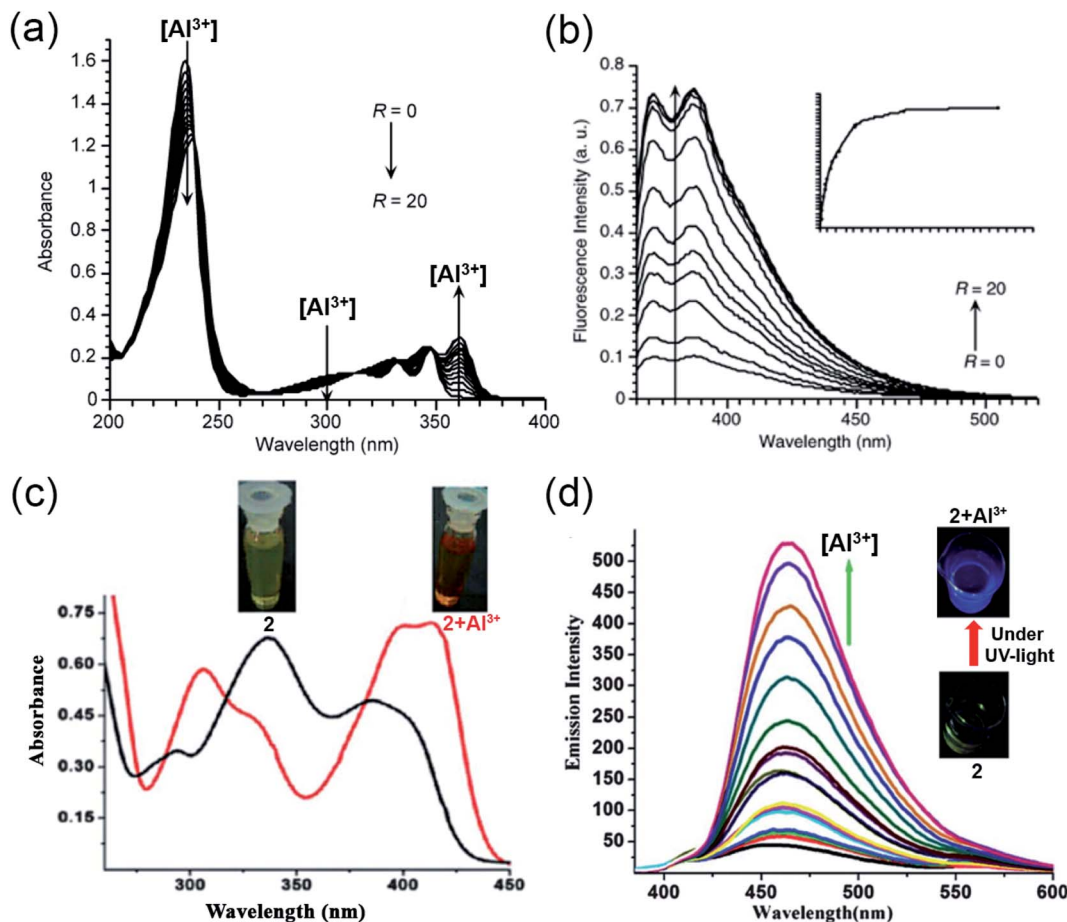


Fig. 3 (a and b) represent the absorption and emission spectra for compound 1 with Al<sup>3+</sup>,  $R = [\text{Al}^{3+}]/[\text{1}]$  in the range  $R = 0$  to 20 at pH =  $3.9 \pm 0.2$ ,  $\lambda_{\text{ex}} = 360$  nm. (c) Absorption spectra of 2 with Al<sup>3+</sup>; the inset displays the visible color change from yellow to reddish-yellow, (d) emission spectra of 2 (12.5  $\mu\text{M}$ ) with different concentrations of Al<sup>3+</sup> in HEPES buffer (DMSO/water: 1/100) of pH = 7.4 at 25 °C; the inset exhibits the blue color of the complex under UV-light illumination (a and b) were reprinted with permission from ref. 45 copyright 2004. Springer Nature, and (c and d) were reprinted with permission from ref. 46 copyright 2012. Royal Society of Chemistry.

310 nm (Fig. 5a) with the concomitant color change of the solution from light yellow to colorless. Concentration-dependent fluorometric titration of aluminium ion (0–2 equiv.) with 5 (10  $\mu\text{M}$ ) in HEPES buffer (pH = 7.0) converted the non-fluorescent probe 5 into a blue fluorescent probe. Fig. 5b demonstrates that the developed chemosensor is highly selective to Al<sup>3+</sup> over other metal ions with a detection limit of 0.1  $\mu\text{M}$ . The large association constant  $1.19 \times 10^8 \text{ M}^{-1}$  indicated the strong metal–ligand interaction. Further, <sup>1</sup>H NMR experiments were carried out to investigate the coordinating site of Al<sup>3+</sup> in the ligand. Interestingly, chemical shifts revealed the ability of three hydroxyl groups of tris to ligate with the aluminium ion forming a 1 : 1 complex. Unlike the previous reports, imine nitrogen and hydroxyl moiety on the naphthalene ring did not participate in forming the Al<sup>3+</sup> chelated product. The switch-on mechanism of fluorescence emission was attributed to the blockage of the PET mechanism in the 5-Al<sup>3+</sup> complex.

Inspired from the hard acid–hard base concept in Al<sup>3+</sup> sensing, in 2017, Yeap and coworkers designed a promising chemosensor 6 that can solely be used in pure water (Fig. 6a).<sup>50</sup>

The probe 6 was incorporated with the –COOH acid moiety, which acts as a hard base and provides good water solubility. Fig. 6b exhibits the UV-Vis spectral changes of 6 with Al<sup>3+</sup>. The gradual addition of Al<sup>3+</sup> to the aqueous solution of the probe enhances the emission intensity at 575 nm through the CHEF mechanism (Fig. 6c). Synthesized probe 6 was highly selective to Al<sup>3+</sup> even in the presence of other metal ions (Fig. 6d). The association constant obtained by the fluorescence titration for the 6-Al<sup>3+</sup> complex is  $0.21 \times 10^2 \text{ M}^{-2}$ . Further, Job's plot analysis and <sup>1</sup>H NMR titration experiments were performed to understand the binding stoichiometry and mode of interaction (Fig. 6e). It was noticed that the coordination of two oxygen atoms of the carboxylic group, two phenolic oxygen atoms, and two oxygen atoms of the oxymethylene group of the ligand with Al<sup>3+</sup> resulted in the formation of the 2 : 1 (6 : Al<sup>3+</sup>) complex (Fig. 6a).

## 2.2 Julolidine and quinoline-based sensors

The water-soluble julolidine-based imine probes have grabbed immense attention from the scientific community owing to their selective determination of aluminium ions in the

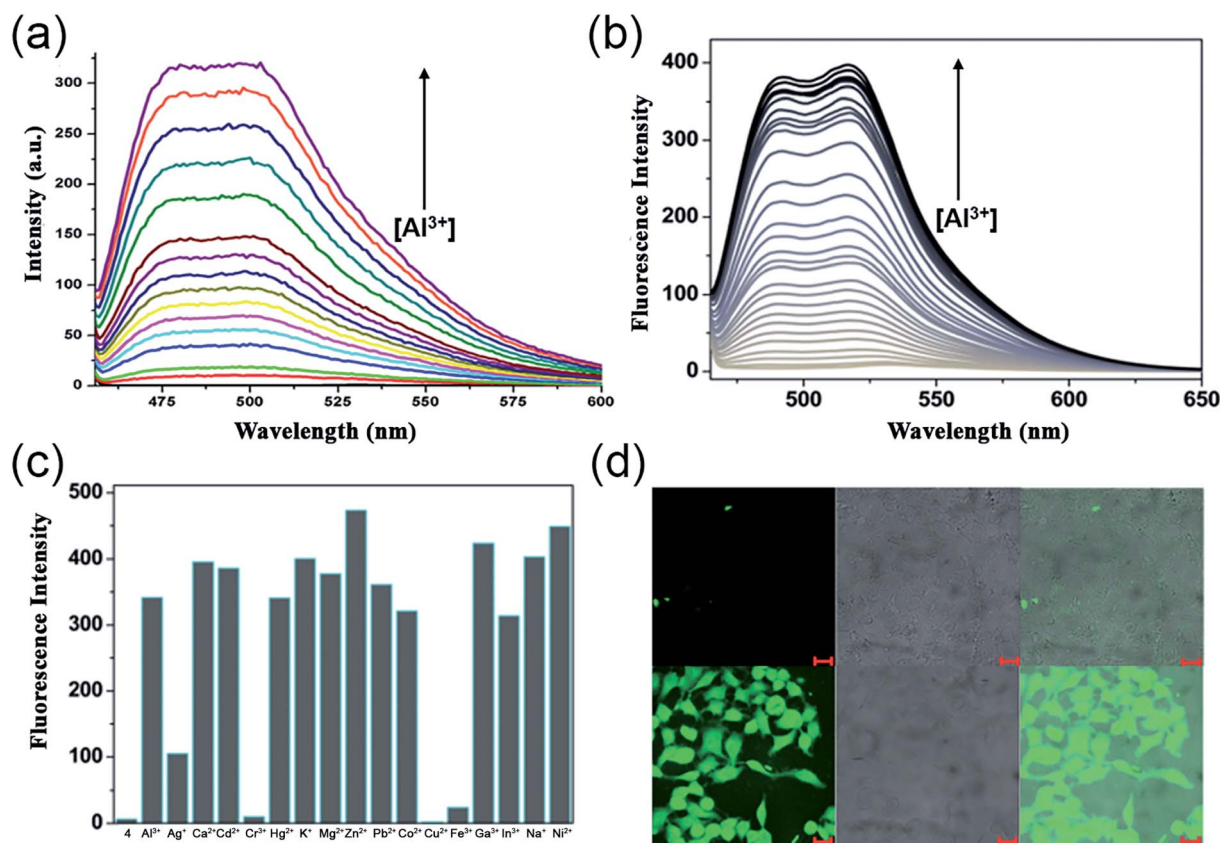


Fig. 4 (a) Fluorescence spectra of **3** (20  $\mu$ M) with 2 equiv. of  $\text{Al}^{3+}$ ,  $\lambda_{\text{ex}} = 450$  nm,  $\lambda_{\text{em}} = 490$  nm, (b) variation in emission intensity of **4** (10  $\mu$ M) upon  $\text{Al}^{3+}$  addition in 50 mM bis-tris buffer [ $\text{Al}^{3+}$ ] = 0–0.6 mM,  $\lambda_{\text{ex}} = 450$  nm, (c) emission response of **4** (10  $\mu$ M) toward  $\text{Al}^{3+}$  ion (34  $\mu$ M) addition in the absence and presence of other metal ions (34  $\mu$ M), (d) fluorescent images of HeLa cells; the above three images were obtained by only incubating with **4**, the bottom images were obtained by incubating with 1 mM  $\text{Al}(\text{NO}_3)_3$  and 10  $\mu$ M of **4**. Left panel shows fluorescent images ( $\lambda_{\text{ex}} = 480$  nm,  $\lambda_{\text{em}} = 520$  nm), middle panel DIC images and right panel merge images (a) was reprinted with permission from ref. 47 copyright 2013. Elsevier, and (b–d) were reprinted with permission from ref. 48 copyright 2014. Royal Society of Chemistry.

biological system. The imine group attached to julolidine is very fluorescent in the rigid form but  $\text{C}=\text{N}$  isomerization causes quenching due to its flexibility (Fig. 7a). This phenomenon has been exploited by researchers for the selective sensing of aluminium ions. The binding of the probe with the metal

provides rigidity to the molecule, which in turn produces a fluorescence response.

J. Y. Noh *et al.* demonstrated the utilization of a Julolidine-based chemosensor for the selective detection of  $\text{Al}^{3+}$  in live-cell imaging.<sup>51</sup> They synthesized the chemosensor *ortho*-

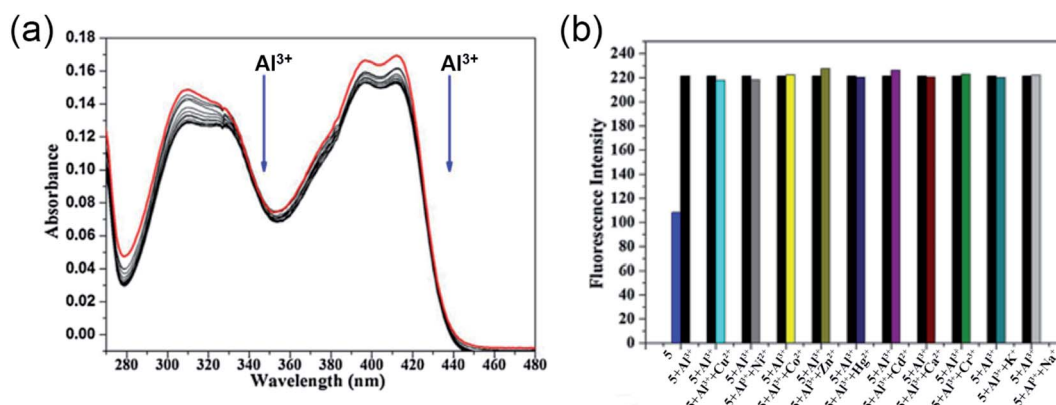


Fig. 5 (a) Absorption spectra of **5** with 0–2 equiv. of  $\text{Al}^{3+}$  in HEPES buffer, (b) the selectivity assay for **5** with other metal ions ( $\text{Na}^+$ ,  $\text{K}^+$ ,  $\text{Ca}^{2+}$ ,  $\text{Cu}^{2+}$ ,  $\text{Zn}^{2+}$ ,  $\text{Cr}^{3+}$ ,  $\text{Cd}^{2+}$ ,  $\text{Co}^{2+}$ ,  $\text{Hg}^{2+}$ ,  $\text{Ni}^{2+}$ ,  $\text{Al}^{3+}$ ) in HEPES buffer (pH = 7.0),  $\lambda_{\text{ex}} = 320$  nm. Reprinted with permission from ref. 49 copyright 2014. Elsevier.



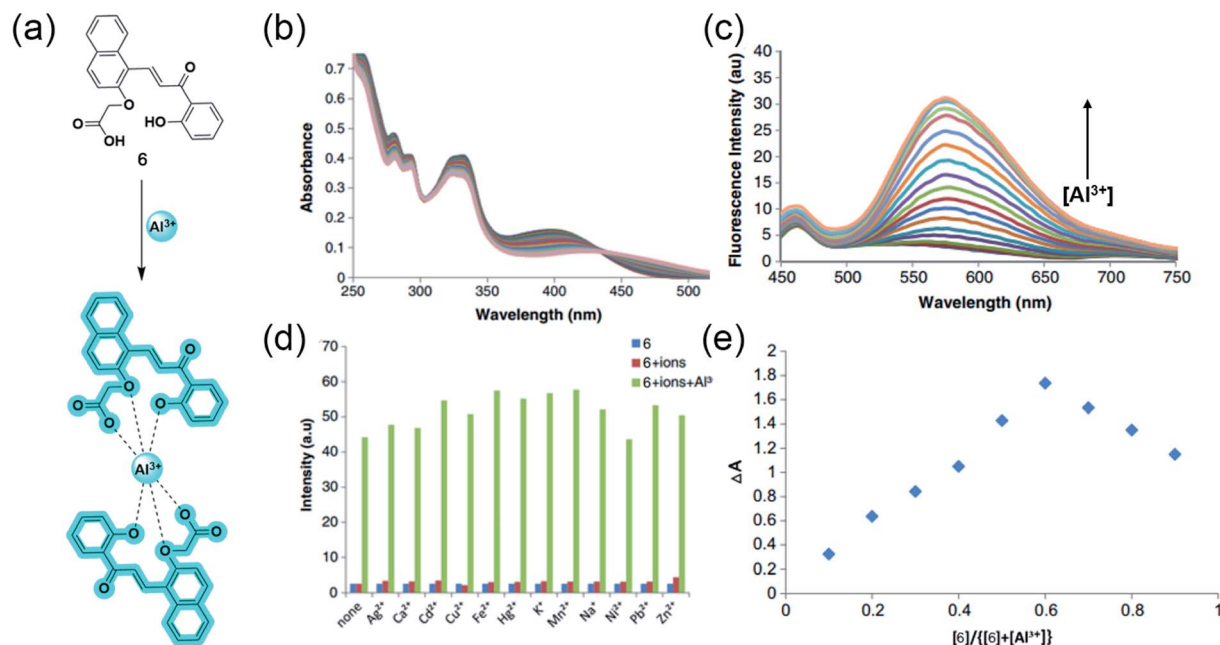


Fig. 6 (a) The structure of chemosensor 6 and the  $\text{Al}^{3+}$  sensing mechanism, (b) and (c) demonstrate the changes in absorption and emission spectra of 6 (100  $\mu\text{M}$ ) with  $\text{Al}^{3+}$ , respectively, (d) Selectivity assay for 6 in the presence of other metal ions, (e) Job's plot showing the 2 : 1 complex of 6 :  $\text{Al}^{3+}$ . Reprinted with permission from ref. 50 copyright 2017. Springer Nature.

phenyljulolidineimine (7) containing the  $\pi$ -conjugated Schiff base using a julolidine-based imine probe (Fig. 7a). The probe showed an excellent turn-on fluorescence response with a 100-fold increase in the fluorescence intensity upon the addition of  $\text{Al}^{3+}$  in an aqueous solution. The 1 : 1 complexation between 7 and  $\text{Al}^{3+}$  was responsible for fluorescence response as it inhibits C=N isomerization and excited-state intramolecular proton transfer (ESIPT) processes. The spectroscopic investigation confirmed the high selectivity and sensitivity for  $\text{Al}^{3+}$  and possessed a detection limit of 0.13  $\mu\text{M}$ . They also demonstrated the application in live-cell imaging, where HeLa cells exposed to 0.1  $\mu\text{M}$   $\text{Al}^{3+}$  were discernible from unexposed cells (Fig. 7d).

In 2016, Y. S. Kim *et al.* further modified the chemosensor and developed 8 by introducing an electron-donating *tert*-butyl group to enhance the solubility in aqueous solution.<sup>52</sup> However, after introducing the *tert*-butyl group, the authors measured a slight increase in the LOD value, but it is still less than 7.41  $\mu\text{M}$ , as recommended by World Health Organization (WHO) in drinking water. Receptor 8 alone has weak fluorescence proposed due to ESIPT involving the phenolic proton. This probe showed a 90-fold enhancement of the emission intensity at 487 nm with  $\text{Al}^{3+}$  treatment (Fig. 7b). This enhancement was proposed due to the chelation-enhanced fluorescence effect, in which the metal ion induces rigidity after chelation and tends to produce fluorescence. Also, C=N isomerization and ESIPT inhibited after chelation leads to fluorescence enhancement. However, the presence of interfering metal ions such as  $\text{Cu}^{2+}$ ,  $\text{Fe}^{2+}$ ,  $\text{Fe}^{3+}$ , and  $\text{Cr}^{3+}$  causes the quenching of the intensity (Fig. 7c). Probe 8 is a suitable and biocompatible sensor for imaging living cells.

As most of the fluorophores reported do not show high selectivity for only the  $\text{Al}^{3+}$  ion, there has always been some

interfering metal ion affecting the fluorescence. Achieving high selectivity and specificity for  $\text{Al}^{3+}$  ion remains a concern for the scientific community. Quinoline-based fluorophores fascinate scientists to overcome this low selectivity of the  $\text{Al}^{3+}$  sensor over the past decade. The ESIPT process in 8-hydroxyquinoline inhibits the fluorescence. Upon binding with the metal ion, the possibility of ESIPT vanishes, which causes turn-on fluorescence. Therefore, researchers well-exploited this phenomenon for aluminium sensing.

In 2017, J. Wang *et al.* reported hydroxyquinoline-based highly selective  $\text{Al}^{3+}$  detection based on a fluorescent chemodosimeter (a system based on analyte-induced irreversible chemical reactions).<sup>53</sup> Compound 9 synthesized by them shows high selectivity with a turn-on fluorescence response to  $\text{Al}^{3+}$  in aqueous solution of 99% water/DMSO (v/v) with a fluorescent enhancement of 582-fold (Fig. 8a and b). The ESIPT process due to intramolecular hydrogen bonding between the hydroxy and the nitrogen of quinoline moiety causes fluorescence quenching in 8-hydroxyquinoline derivatives. After binding with  $\text{Al}^{3+}$ , the intramolecular hydrogen bond broke and gave rise to an enhancement in the fluorescence (Fig. 8e). On the other hand, two reasons for the high selectivity were proposed. First, the binding abilities of other metal ions are weak and cannot form the complex. Second, the paramagnetic nature of metal ions such as  $\text{Cu}^{2+}$ ,  $\text{Ni}^{2+}$ ,  $\text{Co}^{2+}$ , and  $\text{Fe}^{3+}$  will cause fluorescence quenching after binding with the fluorophore. Fluorophore 9 had excellent sensitivity and could detect down to 54  $\text{nmol L}^{-1}$  of  $\text{Al}^{3+}$  (Fig. 8c and f). Another advantage of this fluorophore was the rapid detection of  $\text{Al}^{3+}$  by the naked eye using a fluorescent test paper (Fig. 8d).



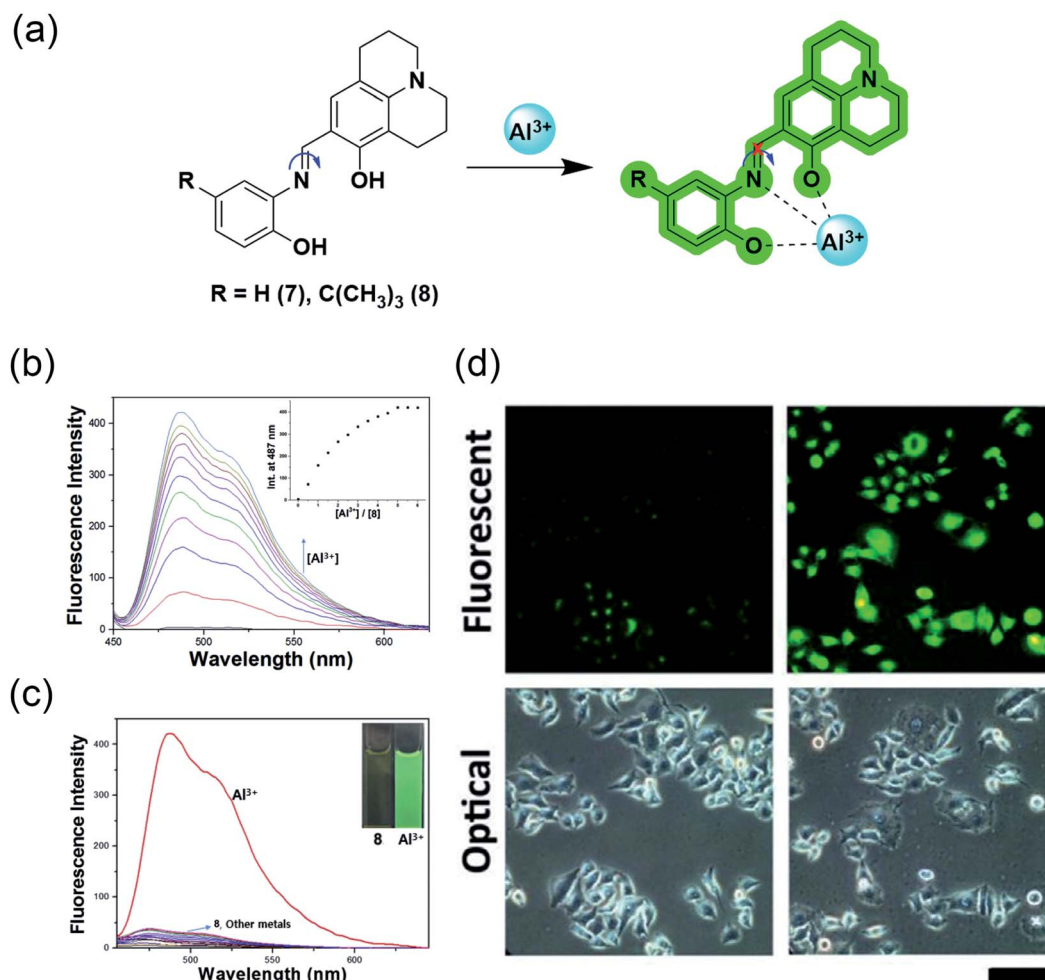


Fig. 7 (a) Sensing mechanism of the julolidine-based probes; (b) fluorescence response of probe **8** to  $\text{Al}^{3+}$  in bis-tris buffer solution; inset: intensity at 487 nm vs. concentration of  $\text{Al}^{3+}$ ; (c) Fluorescence spectra representing the selectivity of probe **8** for  $\text{Al}^{3+}$  over other metal ions in bis-tris buffer solution; (d) observation of changes in the fluorescence intensity in HeLa cells incubated with 0  $\mu\text{M}$  and 100  $\mu\text{M}$  of  $\text{Al}^{3+}$  respectively for 5 h using probe **7** (d) was reprinted with permission from ref. 51 copyright 2013. Elsevier, and (b and c) were reprinted with permission from ref. 52 copyright 2016. Elsevier.

### 2.3 Coumarin and chromone-based $\text{Al}^{3+}$ sensors

Though fluorescent aluminium receptors are reported with various scaffolds, Schiff base sensors hold a strong position because of their flexibility and tunability. Their N and O comprising hard base donor sites provide a favorable coordination sphere for the hard acid  $\text{Al}^{3+}$ , thereby changing the fluorescent properties of probes upon metal binding.<sup>34</sup> Schiff base-based receptors mostly follow the photoinduced electron transfer (PET) mechanism, where the electron transfer from the fluorophore to another part of the probe gets inhibited by the coordination of the metal ion, resulting in an increase in the fluorescence signal by the CHEF effect. Among the Schiff bases, oxygen-containing heterocyclic coumarin and chromone-based fluorophores have received considerable attention for the naked-eye detection of trivalent aluminium cations over the past decades.

Coumarin, an extensively studied fluorophore with high fluorescence quantum yield, visible light emission, and large

Stokes' shift stands out as an excellent skeleton for sensing applications.<sup>55,56</sup> Moreover, comparably less toxicity and ease of modification enable scientists to use coumarin-based aluminium receptors in biological systems. Similarly, chromones are naturally occurring organic molecules with broad pharmacological applications, ranging from anti-inflammatory to anticancer activities. Ideal photophysical and spectroscopic properties of chromones, including strong blue emission, presence of chromophoric  $\text{C}=\text{O}$  and  $\text{C}=\text{C}$  moieties, and small singlet-triplet energy gap have attracted a lot of attention in recent times.<sup>57</sup> Though many coumarin and chromone based aluminium sensors have been reported, their limited bioavailability prevents their use in the detection of aluminium in living systems. Recently, researchers are interested in developing probes by wisely grafting water-soluble moieties such as amino acids and polyalcohols to the fluorophores to exploit them *in vivo*.

In 2015, Qi and coworkers developed a coumarin-based fluorescent 'off-on' aluminium sensor **10** with great water



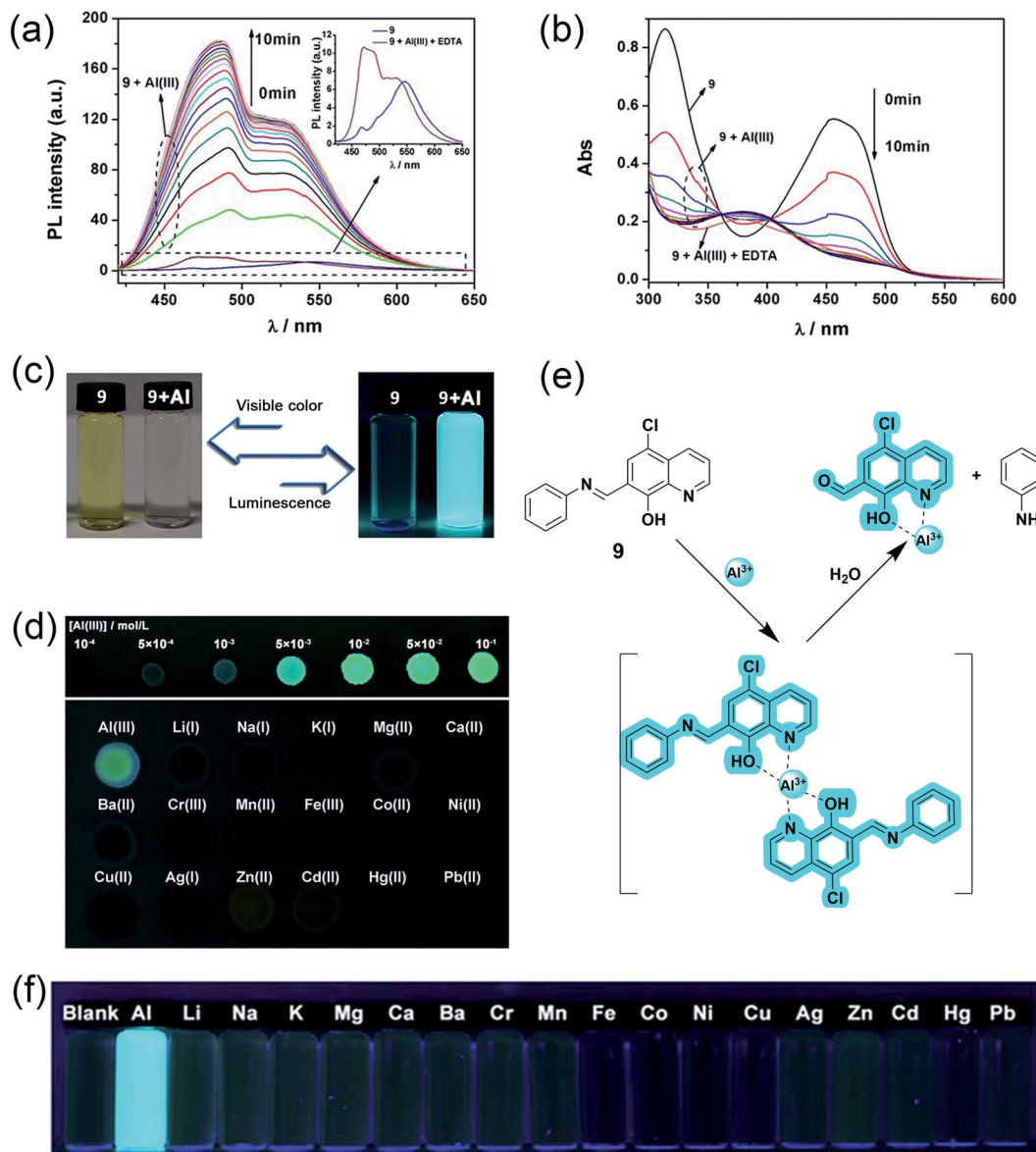


**Fig. 8** (a) Fluorescence spectra and (b) absorption spectra of compound **9** upon the addition Al<sup>3+</sup>. Conditions: 99% water/DMSO (v/v) buffered by 50 mmol L<sup>-1</sup> NaAc-HAc at pH 5.0, the concentrations of **9** and EDTA were 50 μM, and the concentration of Al<sup>3+</sup> was 25 μM, λ<sub>ex</sub> = 403 nm, (c) luminescence and visible color change before and after Al<sup>3+</sup> addition, (d) images of test papers based on **9** for the detection of Al<sup>3+</sup>, (e) proposed mechanism for the interaction between **9** and Al<sup>3+</sup> and, (f) photos of **9** with 1 equivalent of different metal ions. Reprinted with permission from ref. 53 copyright 2017. Wiley-VCH.

solubility attained by attaching an *L*-histidine moiety.<sup>54</sup> Probe **10** having an emission maximum of 445 nm showed excellent selectivity and sensitivity toward aluminium cation even in the presence of other biologically relevant metal ions, except Cu<sup>2+</sup> in physiological conditions (Fig. 9b and c). UV-Vis titration studies, indicating the deprotonation of hydroxyl functionality upon complexation, Job's plot, and ESI-MS studies, suggested a 1 : 1 stoichiometry between the quadridentate ligand and Al<sup>3+</sup>. With the aid of <sup>1</sup>H NMR, authors reasonably propose a sensing mechanism based on the PET phenomenon, where the electron transfer from the Schiff base nitrogen gets inhibited upon metal binding as the lone pairs are no longer available, leading to an

increased fluorescence signal (Fig. 9a). Apart from enhancing the bioavailability, the acid group of *L*-histidine acts as a hard base donor site for metal coordination. Interestingly, **10** also has a greater sensitivity toward Cu<sup>2+</sup> but no fluorescence emission since the complexation does not involve the Schiff base nitrogen and thereby the PET process and the CHEF effect.

Following the line, the same group developed yet another aluminium sensor **11** based on the coumarin-*L*-serine hybrid moiety.<sup>58</sup> The amine part of the Schiff base was sensibly chosen to enhance the water solubility and to provide coordination sites. As Fig. 10b and c suggests, the highly quantum efficient probe exhibited great selectivity toward Al<sup>3+</sup> and Zn<sup>2+</sup>. However,

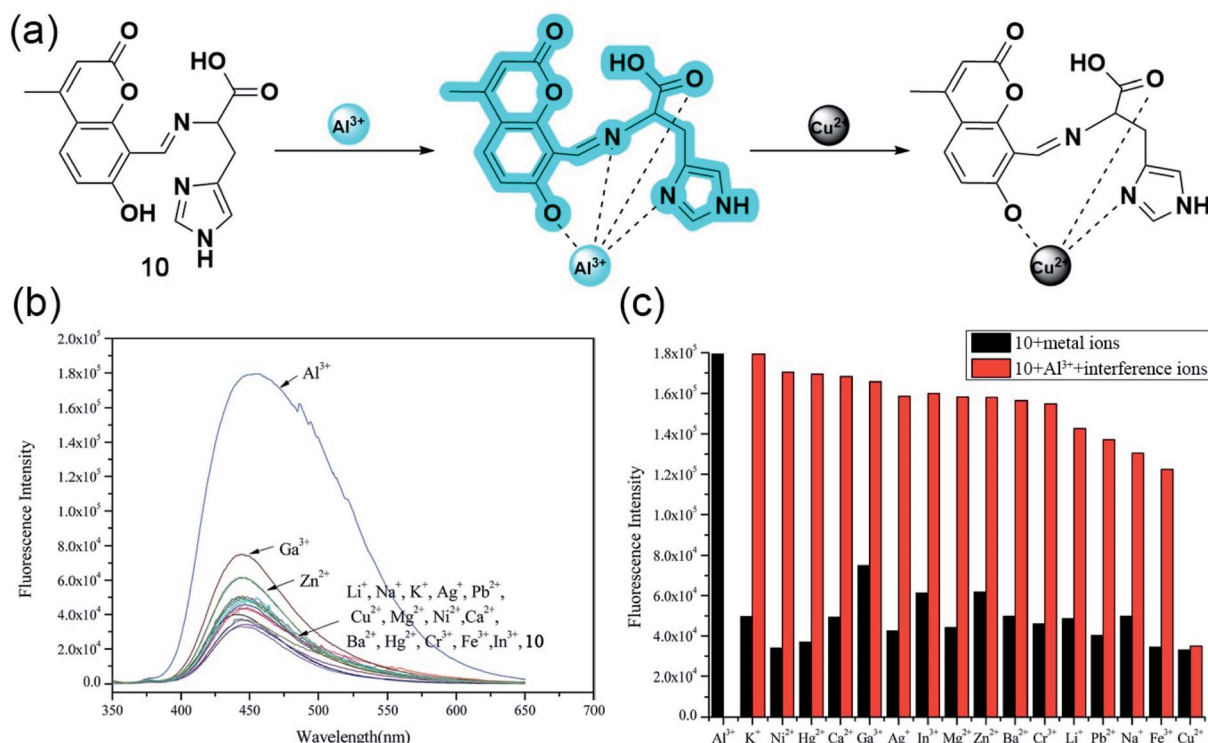


Fig. 9 (a) The proposed mechanism for emission changes of **10** with  $\text{Al}^{3+}$ , and in the presence of  $\text{Cu}^{2+}$ . (b) Fluorescence spectra (10.0 mM,  $\lambda_{\text{ex}} = 334$  nm) with the addition of various metal ions (10.0 equiv.) in aqueous solution (Tris-HCl, 0.1 mM, pH 7.2). (c) Fluorescence intensity of **10** and its complexation with  $\text{Al}^{3+}$  in the presence of various metal ions. Black bar: **10** (10.0 mM) and **10** with 10.0 equiv. of other ions stated. Red bar: 10.0 mM of **10** and 10.0 equiv. of  $\text{Al}^{3+}$  with 10.0 equiv. of metal ions stated ( $\lambda_{\text{ex}} = 334$  nm). Reprinted with permission from ref. 54 copyright 2015. Royal Society of Chemistry.

the interference of other metal ions quenched the fluorescence significantly for the latter in aqueous media (Fig. 10d). The blue emitting 'turn-on' sensor binds with aluminium having a 2 : 1 stoichiometry following the well-explored PET process. Electron transfer from the Schiff base nitrogen and oxygen of L-serine gets repressed upon the coordination of  $\text{Al}^{3+}$ , relapsing the CHEF signal (Fig. 10a).

In 2016, Vladimír Král and coworkers synthesized two novel water-soluble blue-emitting chromone based-Schiff bases having high affinity toward  $\text{Al}^{3+}$  (Fig. 11).<sup>59</sup> The grafting of the polyhydroxylated glucitol moiety improved the bioavailability to a greater extent. The computational studies suggested that **12** can bind to  $\text{Al}^{3+}$  in 1 : 1 ratio, whereas **13** can bind either as 1 : 1 or 2 : 1, the latter being one of the strongest coordination having  $\log(K) = 9.32$ .

Though several coumarin and chromone-based water-soluble aluminium sensors with desirable association constants and detection limits have been developed, their potential bioanalytical applications are seldom investigated.

#### 2.4 Peptide and polymer-based $\text{Al}^{3+}$ sensors

Besides single amino acids, the combination of conjugated fluorophores with short peptides opens up a new arena of ion-selective probes with immense scope in biological systems. The high water-solubility, biocompatibility, structural diversity,

and excellent metal ion binding ability of peptides make them a potential candidate for sensing applications.<sup>60,61</sup> Since hard  $\text{Al}^{3+}$  binds easily with negatively charged oxygen donor groups, amino acids such as Glu, Ser, Asp, or Thr are preferred in peptide-based aluminium receptors.<sup>62,63</sup> On the other hand, the immobilization of conventional small molecular probes onto hydrophilic polymer matrix is also an emerging strategy to develop biocompatible sensors. Similar to peptides, polymers possess desirable characteristic features such as better water solubility, simplicity of use, signal amplification, and ease of fabrication into devices.<sup>64,65</sup> Peptide and polymer-based sensors show exceptional bioavailability and ultrasensitive detection regardless of their bulky structures.

Lee and coworkers reported the first-ever peptide-based water-soluble reversible aluminium sensor **14** in 2016 by grafting a tripeptide (Ser-Glu-Glu) with dansyl fluorophore bearing a sulfonamide group, which can act as a ligand for hard metal ions (Fig. 12a).<sup>66</sup> Emission studies revealed that the 'turn-on' probe has excellent sensitivity toward  $\text{Al}^{3+}$  in acidic aqueous buffered solution with a detection limit in the nanomolar range. The sensing was associated with an eight-fold emission enhancement and a 20 nm blue shift (536 nm to 516 nm), resulting in a color change from yellow to bright green under UV light (Fig. 12b and c). However, the detection ability was pH dependent within the range of 4–7 and a maximum at pH = 5.5. Job's plot and ESI-MS confirm the 1 : 1 stoichiometry along with



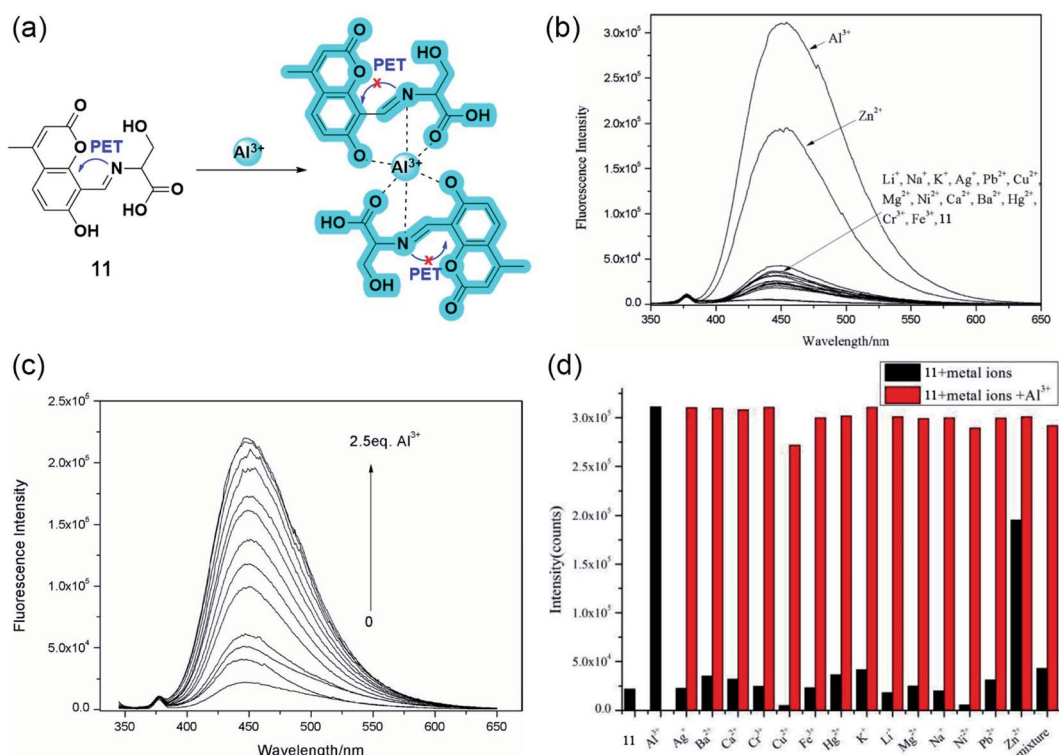


**Fig. 10** (a) The plausible binding mode of **11** with  $\text{Al}^{3+}$  and fluorescence mechanism of the PET processes. (b) Fluorescence spectra (10.0  $\mu\text{M}$ ,  $\lambda_{\text{ex}} = 335 \text{ nm}$ ) with the addition of various metal ions (10.0 equiv.) in aqueous solution (Tris–HCl, 10 mM, pH 7.2). (c) Fluorescence spectra (10.0  $\mu\text{M}$ ,  $\lambda_{\text{ex}} = 335 \text{ nm}$ ) upon the titration of  $\text{Al}^{3+}$  (0–2.5 equiv.) in aqueous solution (Tris–HCl, 10.0 mM, pH 7.2). (d) Fluorescence responses (10.0  $\mu\text{M}$ ,  $\lambda_{\text{ex}} = 335 \text{ nm}$ ) to various metal ions (10.0  $\mu\text{M}$ ) (black column) (10 equiv.) and upon the subsequent addition of  $\text{Al}^{3+}$  (red column) in aqueous solution (Tris–HCl, 10 mM, pH 7.2). Reprinted with permission from ref. 58 copyright 2015. Japan Society for Analytical Chemistry.

the indication of carboxyl group deprotonation upon complexation. The downfield shifts of protons of  $\alpha$ -carbons in  $^1\text{H}$  NMR suggests a quadra-coordinating binding mode where the hydroxyl and carboxyl group of tripeptide and sulfonamide group of dansyl moiety contribute in  $\text{Al}^{3+}$  chelation.

Following the same line, Ramezani and coworkers improved the detection ability by replacing the dansyl probe with more water-soluble and cheaper 2-aminobenzoyl moiety, keeping the tripeptide the same to give **15**.<sup>67</sup> The authors designed another chemosensor **16** with the same fluorophore

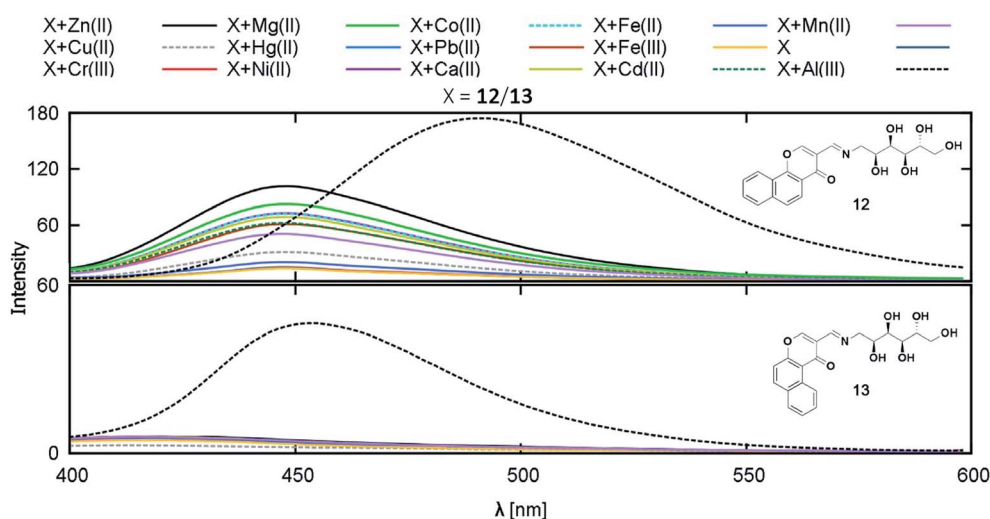


**Fig. 11** Fluorescence response of compounds **12** and **13** on addition of the selected cations. Reprinted with permission from ref. 59 copyright 2017. Taylor & Francis Academic Journals.



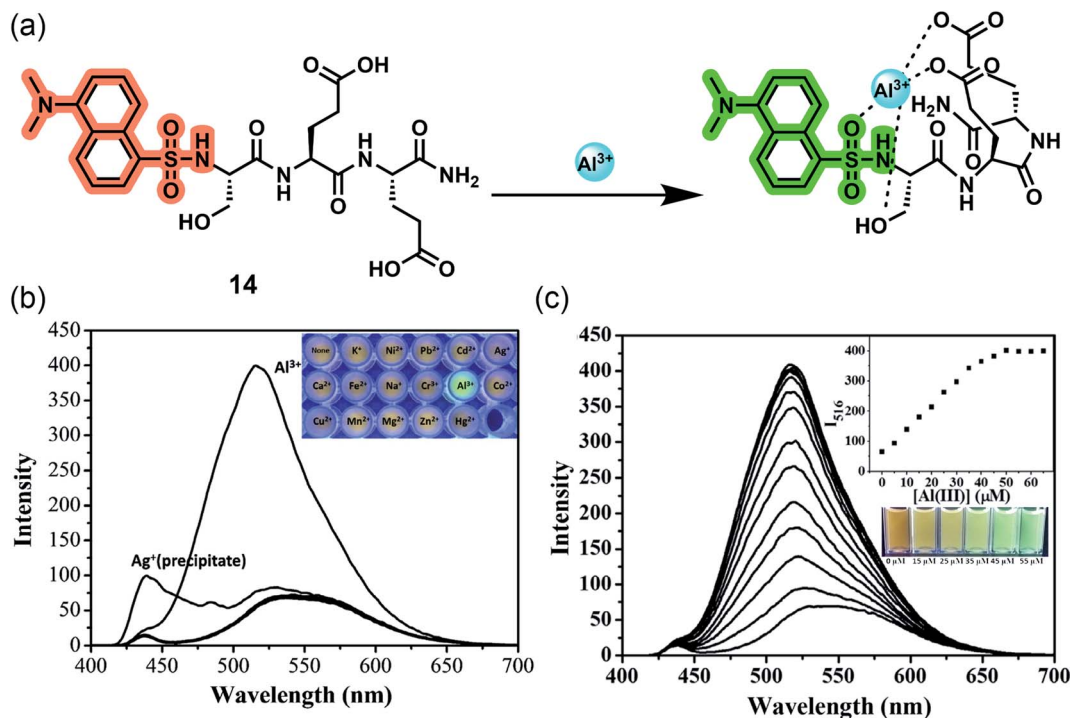


Fig. 12 (a) The proposed binding mode of **14** with  $\text{Al}^{3+}$ . (b) Fluorescence emission spectra of **14** (10  $\mu\text{M}$ ) in the presence of 5 equiv. of various metal ions in aqueous buffered solution (10 mM hexamine, pH 5.5) ( $\lambda_{\text{ex}}$  = 380 nm, slit = 12/8 nm, 430 nm cut off). (c) Fluorescence emission spectra and visible emission color change (inset) of **14** (10  $\mu\text{M}$ ) in aqueous buffered solution (10 mM hexamine, pH 5.5) with increasing concentration of  $\text{Al}^{3+}$  ( $\lambda_{\text{ex}}$  = 380 nm, slit = 12/8 nm, 430 nm cut off). Reprinted with permission from ref. 66 copyright 2016. Elsevier.

based on the heptapeptide sequence Ala–Glu–Pro–Glu–Ala–Glu–Pro, a naturally occurring *Apidaecin 1* gene peptide with three glutamic acids, which can potentially act as ligating sites for  $\text{Al}^{3+}$ . Both turn-on fluorescent sensors are highly specific and selective to  $\text{Al}^{3+}$  in water with emission maxima at 475 nm after complexation (Fig. 13c and d). Similar to **14**, these sensors are also sensitive to pH, working efficiently between pH 4–7, and the 1 : 1 ion binding brings a prominent blue shift of 20–23 nm (Fig. 13e and f). A deeper investigation with the aid of spectroscopic techniques deciphered the ‘off-on’ mechanism based on ICT. 2-Aminobenzoyl moiety act as the electron donor, whereas the amide group of the first amino acid attached to the donor, acts as the electron-withdrawing moiety and binds to the guest cation, lowering the HOMO–LUMO energy gap and facilitating ICT, thereby giving fluorescence enhancement (Fig. 13a and b).

In 2019, Wang and coworkers reported three polymer-based highly selective and sensitive ‘turn-on’  $\text{Al}^{3+}$  sensors by incorporating conventional Schiff base fluorophores onto the non-toxic, biocompatible, water-soluble polyethylene glycol (PEG) matrix.<sup>68–70</sup> The one-step esterification of benzoylhydrazine Schiff base derivative with carboxylated PEG yielded **17** with a 1 : 1 stoichiometry and an excited state intramolecular proton transfer (ESIPT)-based sensing mechanism upon complexation. The chelation of  $\text{Al}^{3+}$  stops the  $\text{C}=\text{N}$  isomerization and restricts the ESIPT process, making the complex rigid and thereby enhancing fluorescent intensity to a greater extent (Fig. 14a). While the grafting of PEG with naphthol- and salicylidene-based Schiff bases resulted in **18** and **19**, respectively, which

binds with  $\text{Al}^{3+}$ , having a 2 : 1 ratio. Both sensors were non-fluorescent in their free state due to the photoinduced electron transfer (PET) from imine to naphthalene or benzene rings, but the rigidity arising from complexation prevents the process, resulting in a bright blue/cyan emission (Fig. 14b and c). All three sensors could detect  $\text{Al}^{3+}$  even in the presence of other highly concentrated analytes, with a quick response time below 20 seconds over a wide range of pH from 5 to 10 (Fig. 14d–i). The reversible recognition property makes them monomolecular circuits, exhibiting an INHIBIT type logic gate with  $\text{Al}^{3+}$  and EDTA (displaces  $\text{Al}^{3+}$ , thereby halting the fluorescence) as the two chemical inputs and the emission intensity at the maxima as the output (Fig. 14k). Sensors **17** and **19** could also give promising results in the naked-eye detection of  $\text{Al}^{3+}$  in real water samples using test strips (Fig. 14j and l).

## 2.5 Nanomaterials-based $\text{Al}^{3+}$ sensors

Nanomaterials-based sensing platforms are gaining immense attention. In this direction, plasmonic, semiconductor-based, and carbonaceous nanoparticles are mostly getting preference compared to other metal oxide nanoparticles. Generally, the plasmonic band of the novel metals displays a visible color due to the interaction of free electrons on metals and electromagnetic fields. Most importantly, the optical absorption property of plasmonic particles is sensitive to the local dielectric of the surrounding medium. Such environment-sensitive plasmonic properties of the most frequently utilized copper, silver, and gold nanoparticles have shown a great promise for sensing



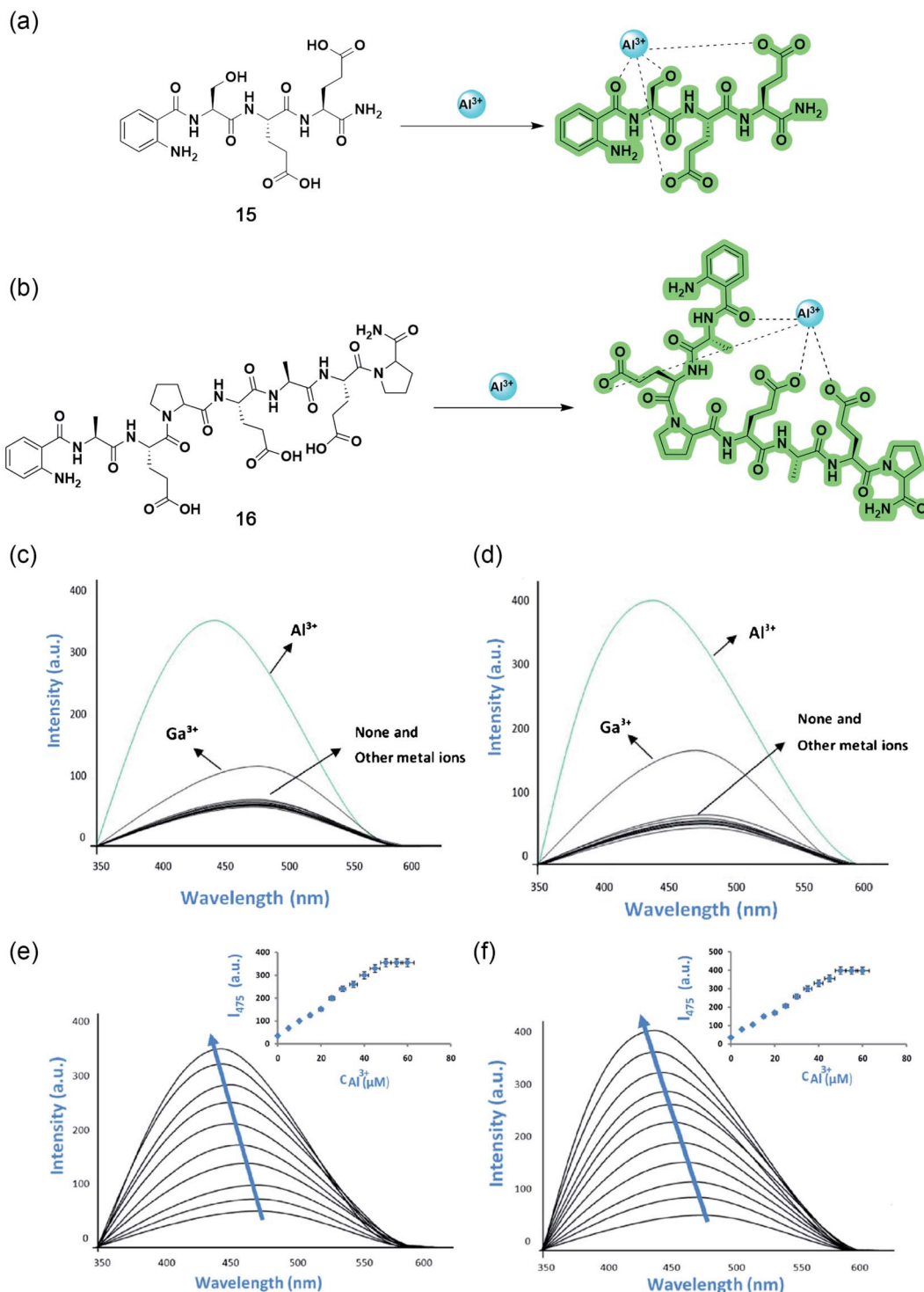
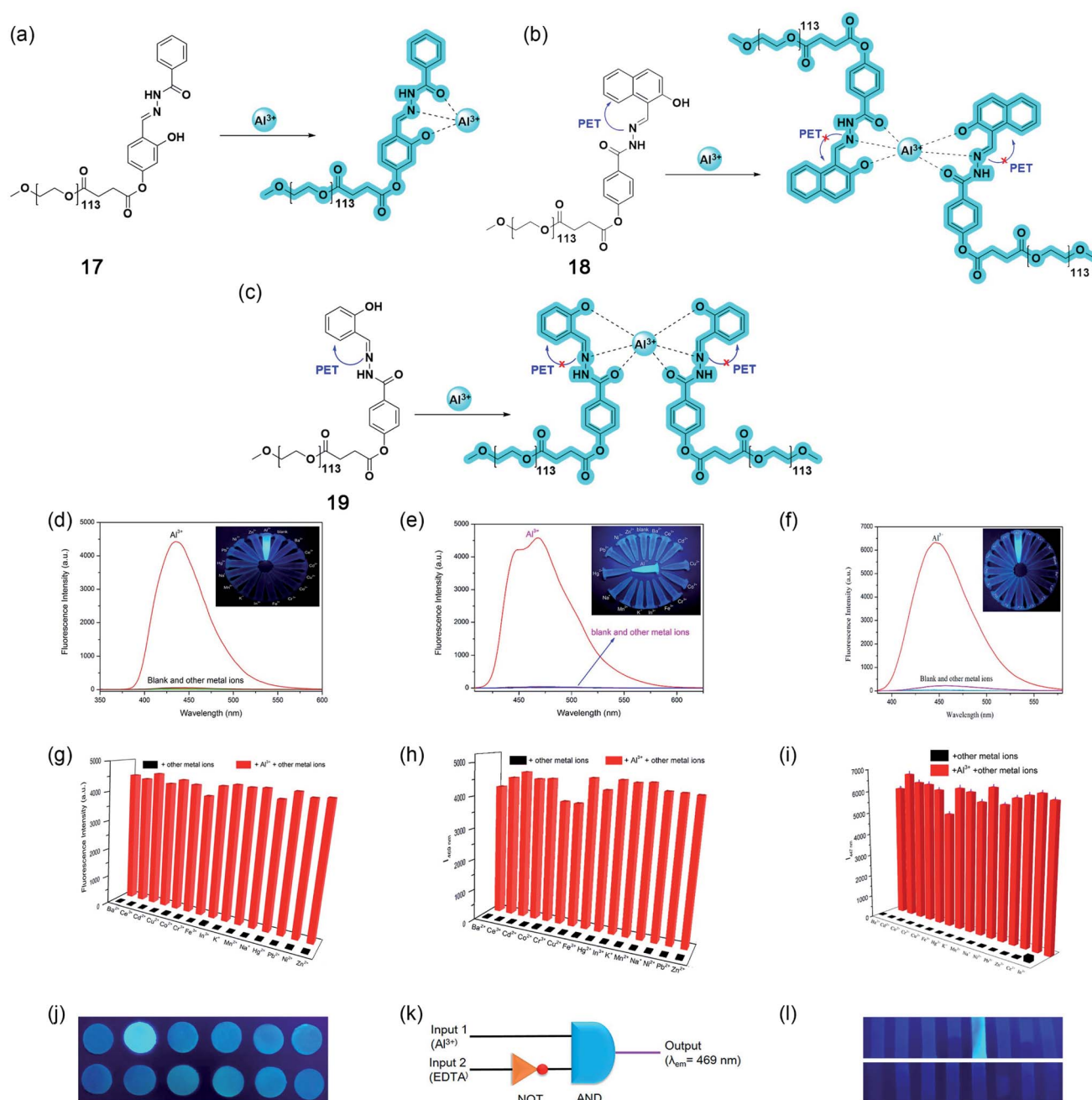


Fig. 13 Structures and proposed binding modes of 15 (a) and 16 (b). Fluorescence responses of 10  $\mu\text{M}$  of 15 (c) and 16 (d) to metal ions in the presence of 5 equiv. of various metal ions by an excitation wavelength at 315 nm in 10 mM hexamine buffer at pH 5.5. Fluorescence emission spectra of 10  $\mu\text{M}$  of 15 (e) and 16 (f) in 10 mM hexamine buffer with increasing concentrations of  $\text{Al}^{3+}$ . Reprinted with permission from ref. 67 copyright 2021. Springer Nature.

bioanalytes, metal ions, and environmentally important small molecules. On the other hand, semiconductor-based luminescent nanoparticles, popularly known as quantum dots, are also employed for sensing applications. In the latter case, the turn

on-off or ratiometric responses are utilized for designing the sensing platform.

In 2013, Wu and coworkers have developed a sensing method for  $\text{Al}^{3+}$  in water at pH 7.4 utilizing silver nanoparticles



**Fig. 14** Structures and proposed binding modes of **17** (a), **18** (b), and **19** (c). Fluorescence spectra of  $10 \mu\text{M}$  **17** (d), **18** (e), and **19** (f) in the presence of various metal ions (2 equiv.) in aqueous solution. Inset: The photograph of **17**, **18**, and **19** with various metal ions (2 equiv.) in aqueous solution under a 365 nm UV lamp. Competition analysis of  $10 \mu\text{M}$  **17** (g), **18** (h), and **19** (i) to various metal ions in aqueous solutions. The black bars represent the intensity when mixed with 2 equiv. of other metal ions; the red bars represent the intensity when mixed with 2 equiv. of  $\text{Al}^{3+}$  and 2 equiv. of other metal ions. (j) Fluorescent detection of  $\text{Al}^{3+}$  using **17** by test paper under a 365 nm UV lamp after being immersed in different aqueous solutions ( $10^{-4} \text{ M}$ ) (from left to right, up: blank,  $\text{Al}^{3+}$ ,  $\text{Co}^{2+}$ ,  $\text{Cr}^{3+}$ ,  $\text{Cu}^{2+}$ , and  $\text{Fe}^{3+}$ ; down:  $\text{Hg}^{2+}$ ,  $\text{Mn}^{2+}$ ,  $\text{Na}^{+}$ ,  $\text{Ni}^{2+}$ ,  $\text{Pb}^{2+}$ , and  $\text{Zn}^{2+}$ ). (k) The monomolecular circuit for the INHIBIT logic gate. (l) Photographs of **19** test strips under a 365 nm UV lamp after being dipped into aqueous solutions of different metal ions ( $100 \mu\text{M}$ ) (from left to right, up:  $\text{Ba}^{2+}$ ,  $\text{Ce}^{3+}$ ,  $\text{Cd}^{2+}$ ,  $\text{Co}^{2+}$ ,  $\text{Al}^{3+}$ ,  $\text{Cr}^{3+}$ ,  $\text{Cu}^{2+}$ , and  $\text{Fe}^{3+}$ ; down:  $\text{Hg}^{2+}$ ,  $\text{In}^{3+}$ ,  $\text{K}^{+}$ ,  $\text{Mn}^{2+}$ ,  $\text{Na}^{+}$ ,  $\text{Ni}^{2+}$ ,  $\text{Pb}^{2+}$ , and  $\text{Zn}^{2+}$ ). Reprinted with permission from ref. 68 and 70 copyright 2019. Elsevier.

(Ag-NPs, **20**).<sup>71</sup> The synthesized Ag-NPs were suitably decorated with an  $\text{Al}^{3+}$  binding ligand, namely, 8-hydroxyquinoline-5-sulfonate. Upon the addition of  $\text{Al}^{3+}$  ions, these modified Ag-NPs show a distinct color change from yellow to deep orange as well as a strong enhancement in the fluorescence emission.

The absorption and emission-based titrations showed high nanomolar sensitivity and good selectivity toward  $\text{Al}^{3+}$  ions over other metal ions. Further, the authors determined  $\text{Al}^{3+}$  ions in living mouse myeloma cells *via* fluorescence imaging.



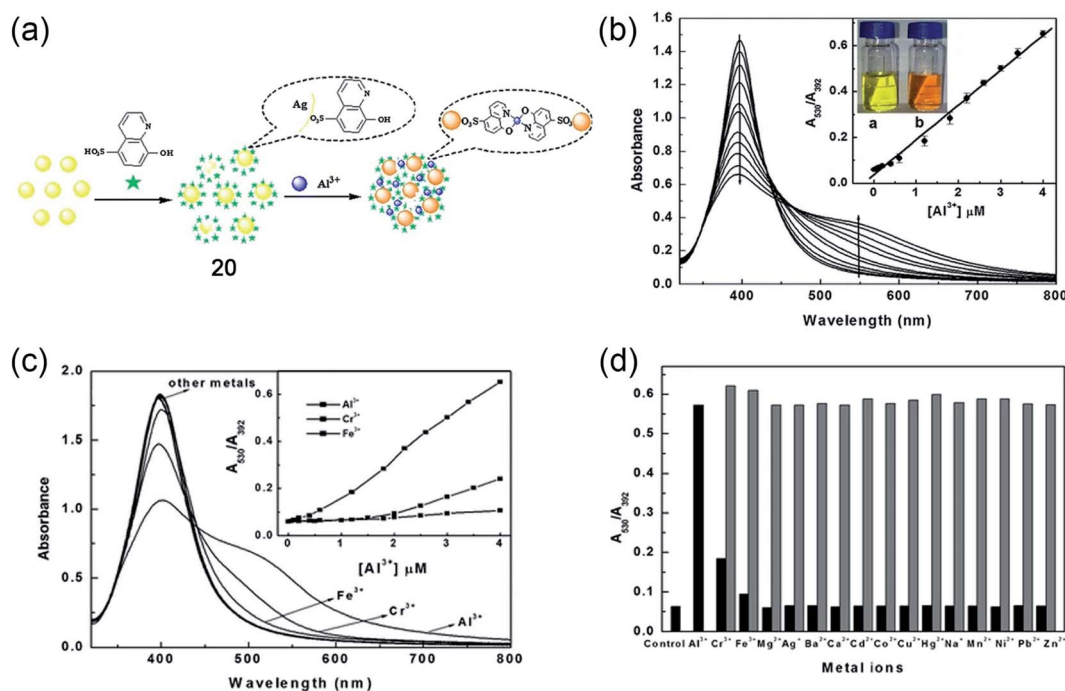


Fig. 15 Silver-nanoparticle (Ag-NPs)-mediated sensing platform (20) for  $\text{Al}^{3+}$  ions in water. (a) Schematic representation of the sensing principle, (b) UV-Vis titration of Ag-NPs with increasing concentration of  $\text{Al}^{3+}$  ions; insets show linear and ratiometric response of optical absorption and color change of the solution before and after the addition of  $\text{Al}^{3+}$  ions, (c) shows the selectivity for  $\text{Al}^{3+}$  ions and the inset shows ratiometric response upon the addition of  $\text{Al}^{3+}$ ,  $\text{Fe}^{3+}$ , and  $\text{Cr}^{3+}$  ions, (d) bar diagram representing the selectivity from the ratiometric optical response for different metal ions. Reprinted with permission from ref. 71 copyright 2013. Springer Nature.

The mechanism of colorimetric and fluorometric detection is associated with the aggregation of Ag-NPs (as shown in Fig. 15a-d) mediated by the 8-hydroxyquinoline-5-sulfonate

ligand, a selective binder for  $\text{Al}^{3+}$ . The authors have observed a ratiometric response in the optical absorption upon the addition of different concentrations of  $\text{Al}^{3+}$ . Such changes in the

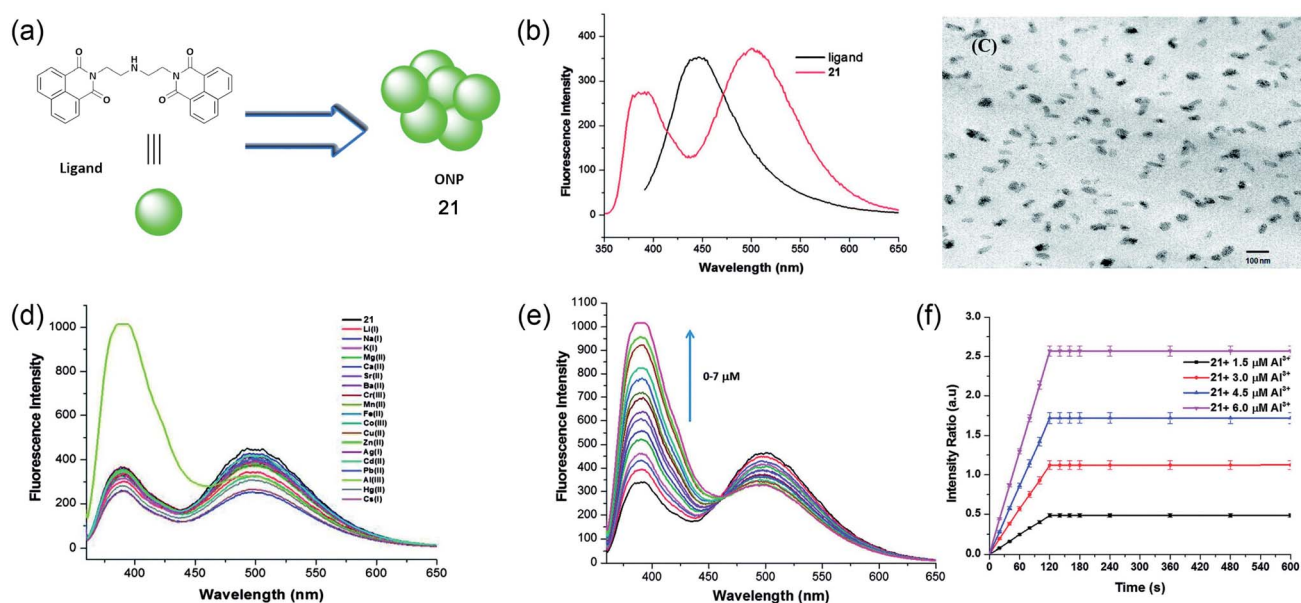


Fig. 16 Water-soluble  $\text{Al}^{3+}$  sensing platform using fluorescent organic nanoparticle 21. (a) Structure of 1,8-naphthalimide ligand used for the synthesis of ONPs, (b) fluorescence properties of 1,8-naphthalimide ligand and self-assembled ONPs, (c) TEM image of ONPs, (d) fluorescence response of ONPs using different metal ions, (e) titration of ONPs with increasing concentration of  $\text{Al}^{3+}$  ions, and (f) kinetic response of fluorescence intensity ratio with different concentration of  $\text{Al}^{3+}$  ions. Reprinted with permission from ref. 72 copyright 2014. Royal Society of Chemistry.



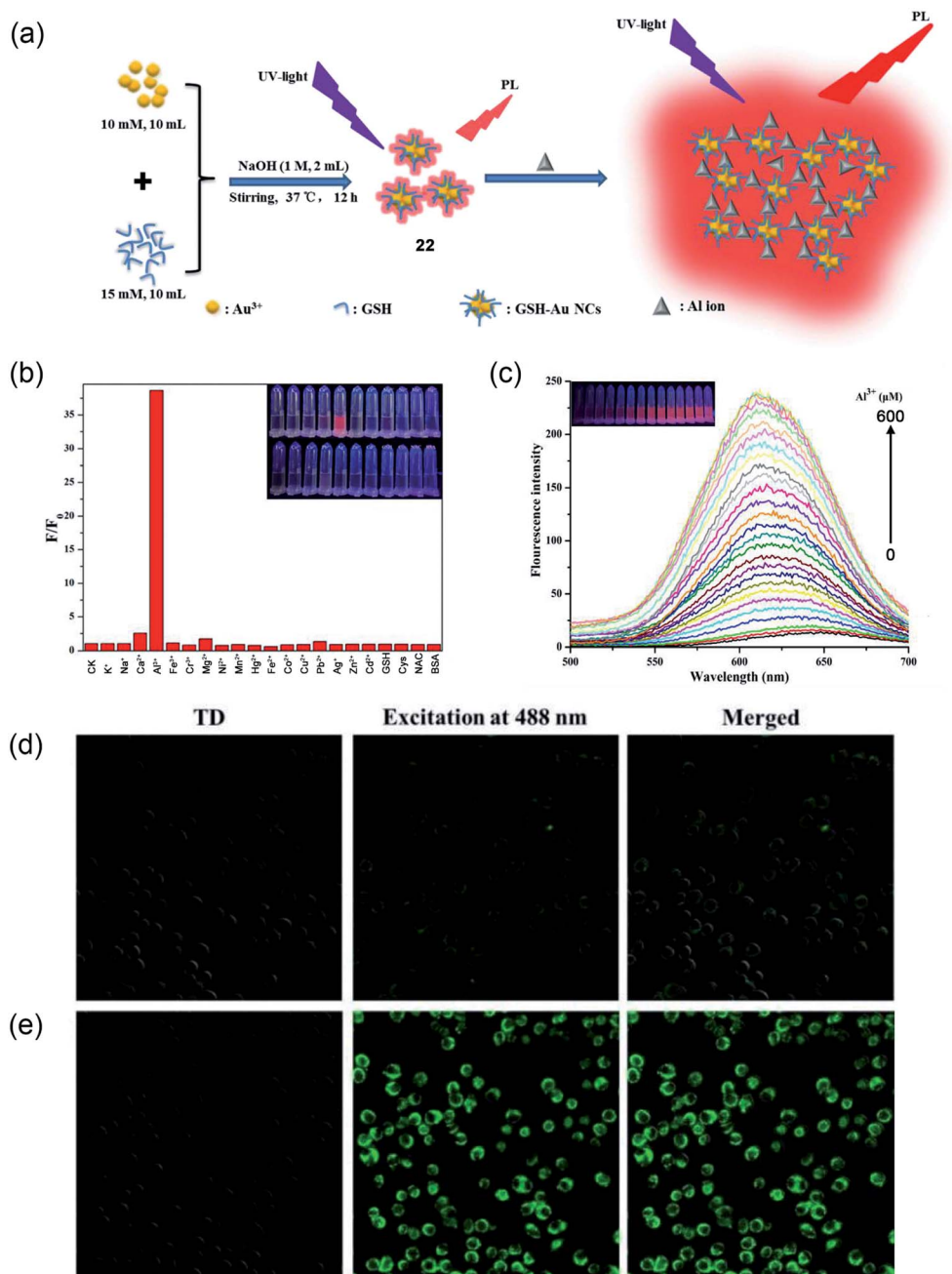


Fig. 17 (a) Schematic illustration of GSH-Au NCs (22) synthesis and the fluorescence enhancement of GSH-Au NCs upon the addition of Al<sup>3+</sup> ion due to the Al<sup>3+</sup>-triggered aggregation of the GSH-Au NCs. (b) Selectivity study of GSH-Au NCs toward Al<sup>3+</sup> against other metal ions, (c) PL emission spectra of GSH-Au NCs solution after adding different concentrations of Al<sup>3+</sup>. Inset: digital photos of different concentrations of Al<sup>3+</sup> processed GSH-Au NCs under UV light. (d and e) Confocal fluorescence images of AT-II cells co-incubated with the as-prepared Au NCs solution without (A) and with (B) 400 μM Al<sup>3+</sup>. Reprinted with permission from ref. 73 copyright 2019. Elsevier.

optical absorption result in a visible color change of the solution. The plasmonic band at 392 nm shifted toward red and a new peak at 530 nm appeared due to the Al<sup>3+</sup>-induced aggregation of Ag-NPs. Upon the addition of Al<sup>3+</sup>, the emission intensity got enhanced by 3 times due to the inhibition of photoinduced electron transfer from the involvement of lone-pair of electrons from the quinolone nitrogen atom due to Al<sup>3+</sup> binding.

Later, in 2014, Kaur and colleagues developed 1,8-naphthalimide-based organic nanoparticles (ONPs, 21) for the sensing of Al<sup>3+</sup> in aqueous media, as shown in Fig. 16a.<sup>72</sup> The molecule itself has an emission maximum at 390 nm in DMF. However, after the formation of ONPs, due to the J-type nano-aggregation, a new peak at 494 nm was observed along the existing peak at 394 nm (Fig. 16b). The morphology and size of ONPs were assessed using TEM and dynamic light scattering



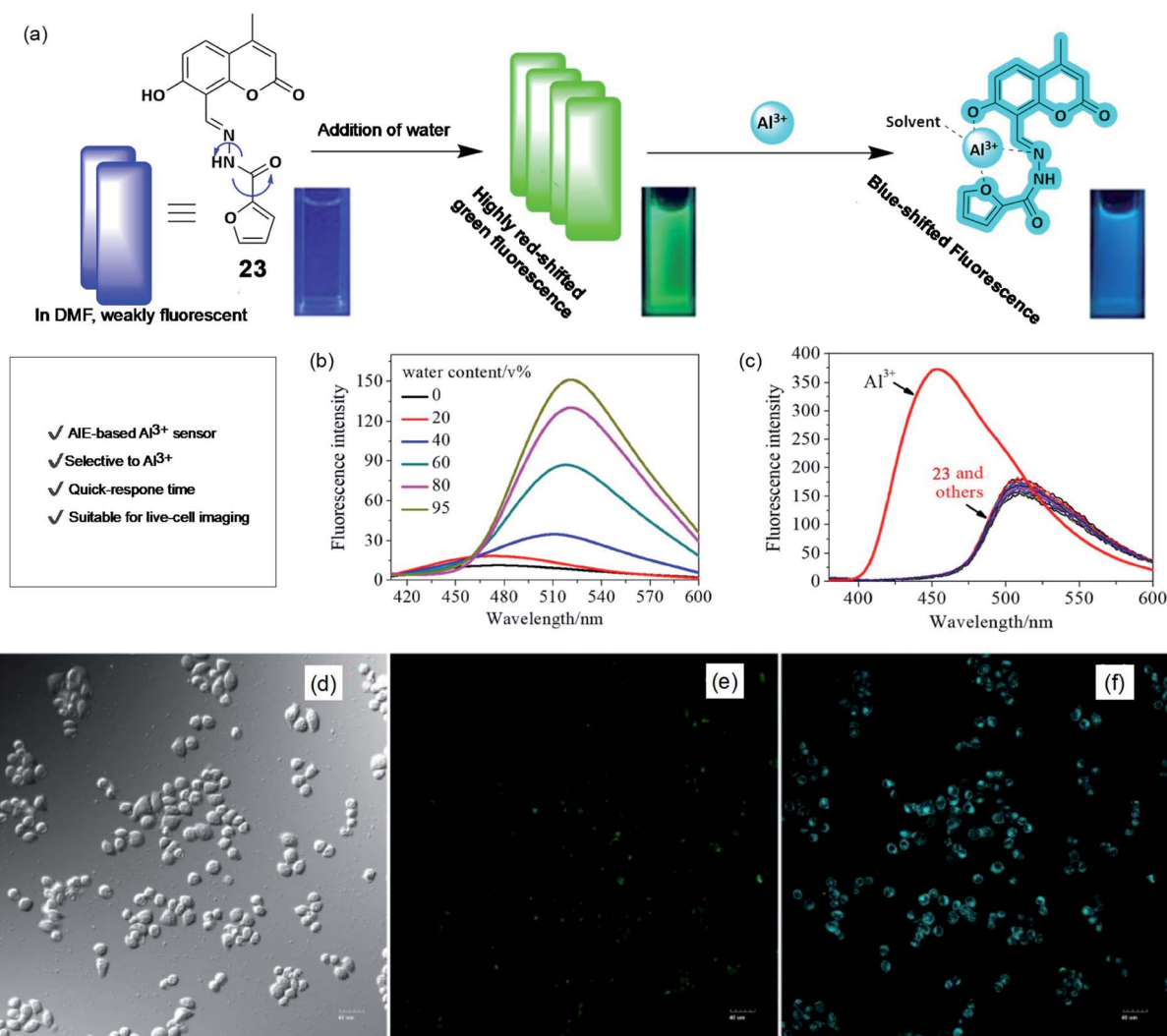


Fig. 18 AIE-based sensing of  $\text{Al}^{3+}$ . (a) Schematically showing the AIE process and  $\text{Al}^{3+}$  sensing. Cuvette picture show fluorescence color change upon AIE and  $\text{Al}^{3+}$  binding. (b) Effect of water addition in DMF solution of the probe causes emission enhancement due to AIE, (c) effect of metal ions on the emission property to show the selectivity toward  $\text{Al}^{3+}$  ions. (d–f) Fluorescence images of A549 cells (d) brightfield, in the presence (f), and absence of  $\text{Al}^{3+}$  (e). Reprinted with permission from ref. 74 copyright 2019. Wiley-VCH.

experiments, respectively. A representative TEM image is shown in Fig. 16c. The developed sensor is highly selective toward  $\text{Al}^{3+}$  and sensitive with a detection limit of  $0.67 \mu\text{M}$ . A significant enhancement of both the emission band was observed upon the addition of only  $\text{Al}^{3+}$  and metal ions have a negligible effect on the emission property (as shown in Fig. 16d and e). The intensity-based kinetic measurement shows a very fast response time of the sensor and within 120 seconds, a saturation of the emission signal was obtained (Fig. 16f). The sensor system was further utilized to determine the  $\text{Al}^{3+}$  content of river water and acidic soil. The fluorescence enhancement of ONPs with the addition of  $\text{Al}^{3+}$  was due to the reduction of photoinduced electron transfer (PET) from the central nitrogen of the diethylenetriamine linker part to electron-deficient  $\text{Al}^{3+}$ . The sensing mechanism was validated using DFT calculation.

Recently, Wang and coworkers presented a fluorescence-based  $\text{Al}^{3+}$  sensing method using thiolated fluorescence

gold nanocluster (Au NCs, 22).<sup>73</sup> The synthetic method was an easy, green, and one-pot synthesis in an aqueous solution. The synthesized GHS-Au NCs were highly stable, ultrasmall, and monodisperse in size with a diameter of 1.4 nm. The large Stokes-shifted emission of GSH-Au NCs shows a fluoro-genic response with  $\sim 40$ -fold enhancement upon binding with  $\text{Al}^{3+}$  (as shown schematically in Fig. 17a). The designed probe has shown a great selectivity for  $\text{Al}^{3+}$  ions and the digital photo at the inset of Fig. 17b also demonstrates the selectivity of  $\text{Al}^{3+}$  ions over other ions in an aqueous solution. The fluorescence intensity of GSH-Au NCs also displays a linear increase in the fluorescence intensity with increasing concentration of  $\text{Al}^{3+}$  from 0–600  $\mu\text{M}$  (Fig. 17c). Furthermore, the authors demonstrated the suitability of the probe for imaging a high concentration of  $\text{Al}^{3+}$  in live cells, as shown in Fig. 17d and e.

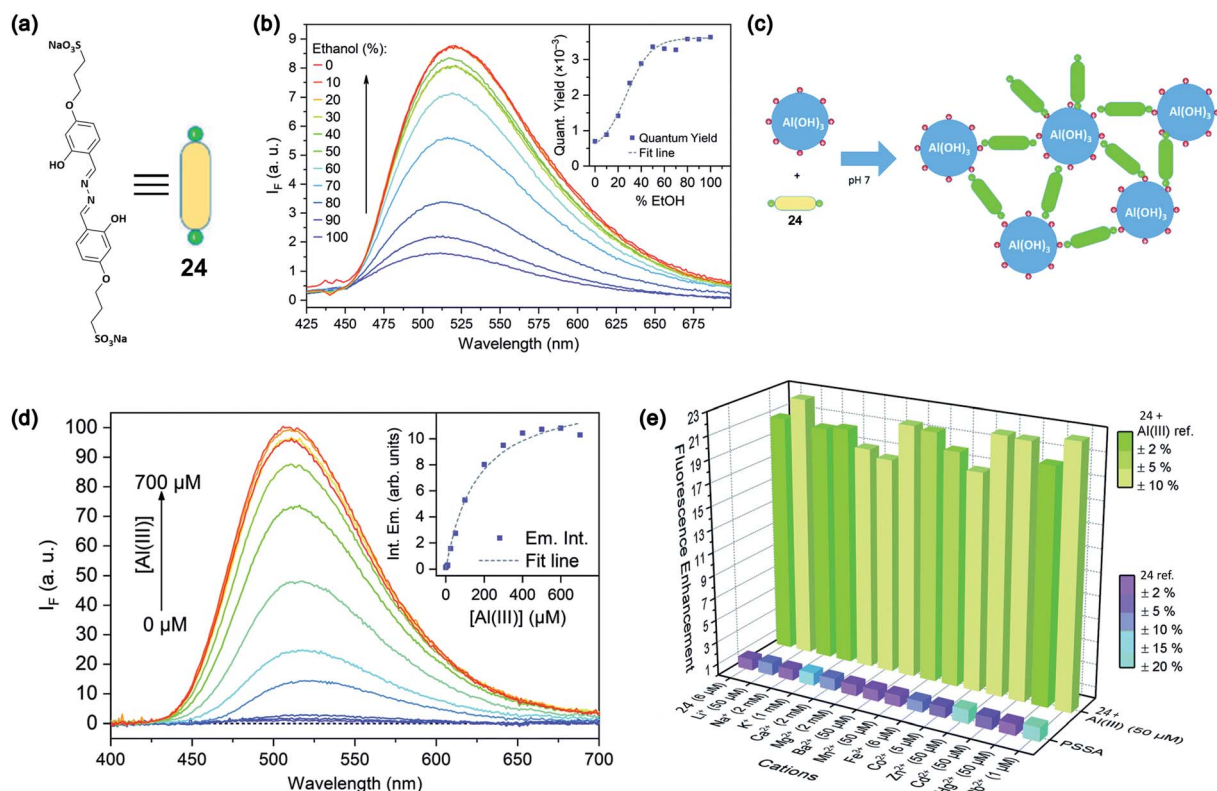


Fig. 19 (a) Structure of PSSA, 24 (b) AIE effect upon the addition of ethanol content; the inset shows the increase in the emission quantum yield with an increasing percentage of ethanol. (c) Schematic representation of the sensing principle. (d) Effect of  $\text{Al}^{3+}$  addition on the emission intensity and the inset shows a plot of intensity variation with increasing concentration of  $\text{Al}^{3+}$  ions. (e) Bar diagram shows the selectivity of detection toward  $\text{Al}^{3+}$  over other metals. Reprinted with permission from ref. 75 copyright 2019. Royal Society of Chemistry.

## 2.6 Water-soluble aggregation induced emission (AIE)-based $\text{Al}^{3+}$ sensors

AIE-based sensing platforms are becoming popular due to their synthetic variation, suitable tunability, and high sensitivity. Recently, in 2019, Li and coworkers have reported a Schiff's base derivative (23), which shows a marked AIE response and specific  $\text{Al}^{3+}$  ion binding property.<sup>74</sup> The weakly-fluorescent Schiff's base compound in DMF turns into a strong green-emissive solution with an emission maximum of about 510 nm upon the addition of more than 40% water (schematically, the AIE process and  $\text{Al}^{3+}$  sensing are demonstrated in Fig. 18a and b). The weak fluorescence emission of probe 23 is due to the fast rotation of the furyl group and C=N isomerization. Upon aggregation, these paths of non-radiative de-activation get restricted and cause a turn-on AIE response. Further, upon the addition of  $\text{Al}^{3+}$  ions in this green-emission solution, the fluorescence emission showed a significant blue shift from 520 nm to 455 nm (as shown in Fig. 18c). The blue-shifted and enhanced emission of the 1 : 1 complexation of probe 23 and  $\text{Al}^{3+}$  is due to restricted intramolecular movements. Other metal ions did not cause any change in the fluorescence emission. This result indicated an excellent specificity for  $\text{Al}^{3+}$  ions over other metal ions. The developed method has very fast response time (within few minutes) and a suitable pH window for  $\text{Al}^{3+}$  detection. As an application of this method, the authors performed live-cell laser

confocal microscopy using A549 lung cancer cells. Cells treated with  $\text{Al}^{3+}$  showed a strong enhancement in the fluorescence emission coming from the cells compared to the same without  $\text{Al}^{3+}$ , indicating good cellular permeability and confirming excellent fluorescence imaging capabilities.

Leray and coworkers in 2019 reported 4-propoxysulfonate salicylaldehyde azine (PSSA, 24)-based water-soluble fluorescent sensor based on the AIE enhancement (AIEE) effect.<sup>75</sup> The structure of PSSA is provided in Fig. 19a. PSSA is highly soluble due to the presence of negatively charged sulfonate groups. However, with increasing concentration of ethanol content, there is a dramatic enhancement of the emission intensity, as shown in Fig. 19b. Upon the addition of  $\text{Al}^{3+}$  ions in PSSA solution, there is a significant *ca.* 100-fold enhancement in the emission intensity due to the complexation-assisted aggregation of PSSA, as schematically shown in Fig. 19c and d. PSSA has also shown good specificity over other metal ions (Fig. 19e) with rapid response time.

## 3. Conclusions

The springing number of optical probes holds promise to overcome the challenges for the effective, convenient, and rapid detection of  $\text{Al}^{3+}$  sensing. Water solubility is the desideratum for efficient fluorescent probes in biological applications. The preceding sections illustrated the different classes of water-





soluble fluorescent sensors to detect  $\text{Al}^{3+}$  in real-time biological application. The strategies used based on PET, ESIPT, C=N isomerization, and CHEF effect are deciphered for the development of turn-on fluorescent probes. This review summarized the findings of several probe's photophysical properties, detection limit, selectivity, and detection mechanism.

Water being the most common medium for the mobilization of aluminium to the biosphere is strictly regulated and quality controlled by health organizations. The Environmental Protection Agency (EPA) and WHO recommend a Secondary Maximum Contaminant Level (SMCL) of  $0.05\text{--}0.2\ \mu\text{g mL}^{-1}$  and  $0.2\ \mu\text{g mL}^{-1}$ , respectively, for aluminium in drinking water.<sup>76</sup> The optical sensors discussed in this review can detect  $\text{Al}^{3+}$  much lower than the SMCL. However, many of them are not utilized for practical applications, and their biocompatibility remains a question to employ in biological systems. Although various probes with certain modifications have been developed, there is still a requirement for highly photostable, selective, and sensitive probes with good aqueous solubility to avoid the usage of mixed aqueous-organic solvent systems. To date, the detection of  $\text{Al}^{3+}$  was achieved in real water samples and live-cell imaging, but clinical utility requires deep tissue and *in vivo* imaging. In this regard, there is significant scope for developing red-emitting fluorescent probes to provide deep tissue penetration depth with negligible autofluorescence. Moreover, interference from other metal ions restricted the exploitation of optical sensors for potential applications in complex biological systems. Future research toward the innovation of highly selective, sensitive, and water-soluble fluorescent probes opens the door for practical applications. The authors believe that this review furnishes in-depth mechanistic information to readers who are fascinated by the emerging field of  $\text{Al}^{3+}$  sensors for biological application.

## Conflicts of interest

There is no conflict of interest to declare.

## Acknowledgements

We wish to acknowledge the financial support from the host institute IISER Bhopal (IISERB). ARUP thanks DST for INSPIRE fellowship during his BS-MS studies at IISERB. KP and AS are thankful to IISER Bhopal and CSIR, respectively, for their doctoral fellowship. The authors also thank Mr Vishnu K for assisting in the design of illustrations.

## References

- 1 E. Monosson, in *Evolution in a Toxic World: How Life Responds to Chemical Threats*, Island Press/Center for Resource Economics, Washington, DC, 2012, pp. 48–64, DOI: [10.5822/978-1-61091-221-1\\_4](https://doi.org/10.5822/978-1-61091-221-1_4).
- 2 C. D. Foy, R. L. Chaney and M. C. White, *Annu. Rev. Plant Physiol.*, 1978, **29**, 511–566.
- 3 M. Schmitt, T. Watanabe and S. Jansen, *AoB Plants*, 2016, **8**, plw065.
- 4 R. A. Yokel, *Neurotoxicology*, 2000, **21**, 813–828.
- 5 C. Poschenrieder, B. Gunse, I. Corrales and J. Barcelo, *Sci. Total Environ.*, 2008, **400**, 356–368.
- 6 E. Bojorquez-Quintal, C. Escalante-Magana, I. Echevarria-Machado and M. Martinez-Estevez, *Front. Plant Sci.*, 2017, **8**, 1767.
- 7 F. P. Veitch, *J. Am. Chem. Soc.*, 2002, **26**, 637–662.
- 8 M. A. Qifu, Z. Rengel and J. Kuo, *Ann. Bot.*, 2002, **89**, 241–244.
- 9 L. V. Kochian, M. A. Pineros and O. A. Hoekenga, *Plant Soil*, 2005, **274**, 175–195.
- 10 E. Delhaize and P. R. Ryan, *Plant Physiol.*, 1995, **107**, 315–321.
- 11 D. L. Jones, E. B. Blancaflor, L. V. Kochian and S. Gilroy, *Plant Cell Environ.*, 2006, **29**, 1309–1318.
- 12 X. B. Zhang, P. Liu, Y. Yang and G. D. Xu, *Bot. Stud.*, 2007, **48**, 435–444.
- 13 X. J. Zhao, E. Sucoff and E. J. Stadelmann, *Plant Physiol.*, 1987, **83**, 159–162.
- 14 S. Ishikawa and T. Wagatsuma, *Plant Cell Physiol.*, 1998, **39**, 516–525.
- 15 J. W. Huang, D. L. Grunes and L. V. Kochian, *Plant Soil*, 1995, **171**, 131–135.
- 16 E. Olivares, E. Pena, E. Marcano, J. Mostacero, G. Aguiar, M. Benitez and E. Rengifo, *Environ. Exp. Bot.*, 2009, **65**, 132–141.
- 17 I. O. Igbokwe, E. Igwenagu and N. A. Igbokwe, *Interdiscip. Toxicol.*, 2019, **12**, 45–70.
- 18 C. Exley and E. Clarkson, *Sci. Rep.*, 2020, **10**, 7770.
- 19 K. E. Page, K. N. White, C. R. McCrohan, D. W. Killilea and G. J. Lithgow, *Metallomics*, 2012, **4**, 512–522.
- 20 J. Kamalov, D. O. Carpenter and I. Birman, *J. Toxicol.*, 2011, **2011**, 796719.
- 21 S. Biswas, V. Sharma, P. Kumar and A. L. Koner, *Sens. Actuator B-Chem.*, 2018, **260**, 460–464.
- 22 R. Roy, R. Bhowal, V. Sharma, D. Chopra and A. L. Koner, *J. Mater. Chem. C*, 2021, **9**, 1778–1785.
- 23 R. Roy, N. R. Sajeev, V. Sharma and A. L. Koner, *ACS Appl. Mater. Interfaces*, 2019, **11**, 47207–47217.
- 24 P. Kumar, S. Biswas and A. L. Koner, *New J. Chem.*, 2020, **44**, 10771–10775.
- 25 S. Mallick, F. Chandra and A. L. Koner, *Analyst*, 2016, **141**, 827–831.
- 26 A. Silswal, A. Kanojiya and A. L. Koner, *Front. Chem.*, 2022, **10**, 840297.
- 27 D. Das, R. Alam, A. Katarkar and M. Ali, *Photochem. Photobiol. Sci.*, 2019, **18**, 242–252.
- 28 S. Goswami, S. Paul and A. Manna, *RSC Adv.*, 2013, **3**, 10639–10643.
- 29 B. Liu, P. F. Wang, J. Chai, X. Q. Hu, T. Gao, J. B. Chao, T. G. Chen and B. S. Yang, *Spectrochim. Acta A Mol. Biomol. Spectrosc.*, 2016, **168**, 98–103.
- 30 A. Barba-Bon, A. M. Costero, S. Gil, M. Parra, J. Soto, R. Martinez-Manez and F. Sancenon, *Chem. Commun.*, 2012, **48**, 3000–3002.
- 31 S. Goswami, K. Aich, S. Das, A. K. Das, D. Sarkar, S. Panja, T. K. Mondal and S. Mukhopadhyay, *Chem. Commun.*, 2013, **49**, 10739–10741.



- 32 P. Roy, *Dalton Trans.*, 2021, **50**, 7156–7165.
- 33 D. Ezhumalai, I. Mathivanan and A. Chinnadurai, *Spectrochim. Acta A Mol. Biomol. Spectrosc.*, 2018, **199**, 209–219.
- 34 G. Balamurugan, S. Velmathi, N. Thirumalaivasan and S. P. Wu, *Analyst*, 2017, **142**, 4721–4726.
- 35 W. H. Ding, D. Wang, X. J. Zheng, W. J. Ding, J. Q. Zheng, W. H. Mu, W. Cao and L. P. Jin, *Sens. Actuators, B*, 2015, **209**, 359–367.
- 36 A. K. Saini, V. Sharma, P. Mathur and M. M. Shaikh, *Sci. Rep.*, 2016, **6**, 34807.
- 37 H. Tian, X. Qiao, Z. L. Zhang, C. Z. Xie, Q. Z. Li and J. Y. Xu, *Spectrochim. Acta A Mol. Biomol. Spectrosc.*, 2019, **207**, 31–38.
- 38 H. Xiao, K. Chen, N. Jiang, D. Cui, G. Yin, J. Wang and R. Wang, *Analyst*, 2014, **139**, 1980–1986.
- 39 L. Wang, J. Yang, H. Wang, C. Ran, Y. Su and L. Zhao, *Sensors*, 2019, **19**, 2423.
- 40 K. Bakshi and B. K. Pal, *Talanta*, 1994, **41**, 81–87.
- 41 D. P. Roek, J. E. Chateaufneuf and J. F. Brennecke, *Ind. Eng. Chem. Res.*, 2000, **39**, 3090–3096.
- 42 F. P. Schwarz and S. P. Wasik, *Anal. Chem.*, 1976, **48**, 524–528.
- 43 I. H. Hwang, Y. W. Choi, K. B. Kim, G. J. Park, J. J. Lee, L. Nguyen, I. Noh and C. Kim, *New J. Chem.*, 2016, **40**, 171–178.
- 44 J. Jun Lee, G. Jin Park, Y. Sung Kim, S. Young Lee, H. Ji Lee, I. Noh and C. Kim, *Biosens. Bioelectron.*, 2015, **69**, 226–229.
- 45 E. Destandau, V. Alain and E. Bardez, *Anal. Bioanal. Chem.*, 2004, **378**, 402–410.
- 46 S. Sen, T. Mukherjee, B. Chattopadhyay, A. Moirangthem, A. Basu, J. Marek and P. Chattopadhyay, *Analyst*, 2012, **137**, 3975–3981.
- 47 V. P. Singh, K. Tiwari, M. Mishra, N. Srivastava and S. Saha, *Sens. Actuators, B*, 2013, **182**, 546–554.
- 48 S. Kim, J. Y. Noh, S. J. Park, Y. J. Na, I. H. Hwang, J. Min, C. Kim and J. Kim, *RSC Adv.*, 2014, **4**, 18094–18099.
- 49 Z. C. Liu, Y. X. Li, Y. J. Ding, Z. Y. Yang, B. D. Wang, Y. Li, T. R. Li, W. Luo, W. P. Zhu, J. P. Xie and C. J. Wang, *Sens. Actuators, B*, 2014, **197**, 200–205.
- 50 G. Y. Yeap, Y. H. Chan and W. A. K. Mahmood, *J. Fluoresc.*, 2017, **27**, 2017–2022.
- 51 J. Y. Noh, S. Kim, I. H. Hwang, G. Y. Lee, J. Kang, S. H. Kim, J. Min, S. Park, C. Kim and J. Kim, *Dyes Pigm.*, 2013, **99**, 1016–1021.
- 52 Y. S. Kim, J. J. Lee, Y. W. Choi, G. R. You, L. Nguyen, I. Noh and C. Kim, *Dyes Pigm.*, 2016, **129**, 43–53.
- 53 J. Wang, Y. Li, K. Li, X. Meng and H. Hou, *Chem. –Eur. J.*, 2017, **23**, 5081–5089.
- 54 L. Q. Yan, Y. Ma, M. F. Cui and Z. J. Qi, *Anal. Methods*, 2015, **7**, 6133–6138.
- 55 Y. X. Song, Z. Chen and H. Q. Li, *Curr. Org. Chem.*, 2012, **16**, 2690–2707.
- 56 L. Wang, Y. F. Li, G. P. Li, Z. K. Xie and B. X. Ye, *Anal. Methods*, 2015, **7**, 3000–3005.
- 57 M. A. Rohman, P. Baruah, S. O. Yesylevskyy and S. Mitra, *Chem. Phys.*, 2019, **517**, 67–79.
- 58 L. Q. Yan, M. F. Cui, Y. Zhou, Y. Ma and Z. J. Qi, *Anal. Sci.*, 2015, **31**, 1055–1059.
- 59 M. Jakubek, Z. Kejik, V. Parchansky, R. Kaplanek, L. Vasina, P. Martasek and V. Kral, *Supramol. Chem.*, 2017, **29**, 1–7.
- 60 D. Divya and S. Thennarasu, *Spectrochim. Acta A Mol. Biomol. Spectrosc.*, 2020, **243**, 118796.
- 61 P. Wang, L. Liu, P. Zhou, W. Wu, J. Wu, W. Liu and Y. Tang, *Biosens. Bioelectron.*, 2015, **72**, 80–86.
- 62 X. Yang, Q. Zhang, L. Li and R. Shen, *J. Inorg. Biochem.*, 2007, **101**, 1242–1250.
- 63 M. Kilyen, P. Forgo, A. Lakatos, G. Dombi, T. Kiss, N. Kotsakis and A. Salifoglou, *J. Inorg. Biochem.*, 2003, **94**, 207–213.
- 64 H. N. Kim, Z. Guo, W. Zhu, J. Yoon and H. Tian, *Chem. Soc. Rev.*, 2011, **40**, 79–93.
- 65 W. S. P. Carvalho, M. Wei, N. Ikpo, Y. Gao and M. J. Serpe, *Anal. Chem.*, 2018, **90**, 459–479.
- 66 B. In, G. W. Hwang and K. H. Lee, *Bioorg. Med. Chem. Lett.*, 2016, **26**, 4477–4482.
- 67 S. Ramezanpour, H. Barzinmehr, P. Shiri, C. Meier, S. A. Ayatollahi and M. Mehrazar, *Anal. Bioanal. Chem.*, 2021, **413**, 3881–3891.
- 68 L. Bai, G. Li, L. Li, M. Gao, H. Li, F. Tao, A. Deng, S. Wang and L. Wang, *React. Funct. Polym.*, 2019, **139**, 1–8.
- 69 L. Bai, Y. Xu, G. Li, S. Tian, L. Li, F. Tao, A. Deng, S. Wang and L. Wang, *Polymers*, 2019, **11**, 573.
- 70 L. Bai, F. Tao, L. Li, A. Deng, C. Yan, G. Li and L. Wang, *Spectrochim. Acta A Mol. Biomol. Spectrosc.*, 2019, **214**, 436–444.
- 71 Y. Shang, D. Gao, F. Y. Wu and X. F. Wan, *Microchim. Acta*, 2013, **180**, 1317–1324.
- 72 A. Saini, J. Singh, R. Kaur, N. Singh and N. Kaur, *New J. Chem.*, 2014, **38**, 4580–4586.
- 73 P. Luo, Y. Zheng, Z. Qin, C. Li, H. Jiang and X. Wang, *Talanta*, 2019, **204**, 548–554.
- 74 Y. Xie, X. Li, L. Yan and J. Li, *Luminescence*, 2020, **35**, 156–162.
- 75 H. L. Nguyen, N. Kumar, J. F. Audibert, R. Ghasemi, J. P. Lefevre, M. H. Ha-Thi, C. Mongin and I. Leray, *New J. Chem.*, 2019, **43**, 15302–15310.
- 76 I. Krupińska, *Molecules*, 2020, **25**, 641.

